Swiss Journal of Palaeontology (2026) 145: 901–926 | DOI 10.3897/sjp.145.196379

PENSOFT

Swiss Journal of Palaeontology

SGG SGS

scnat swiss academy of sciences

Research Article

A new postcranial skeleton of *Sinovenator changii* (Theropoda, Troodontidae) from the Jehol Biota of the Ningcheng Basin, Inner Mongolia, China

Dongxiang Yu[1,2], Honggang Zhang[3], Chang-Fu Zhou[1], Rui Pei[4]

1 *College of Earth Science and Engineering, Shandong University of Science and Technology, Qingdao, 266590, China*
2 *Hubei Qinglongshan National Nature Reserve of Dinosaur Egg Fossil Group, Shiyan, 442532, China*
3 *Paleontological Museum of Liaoning, Shenyang Normal University, Shenyang 110034, China*
4 *Key Laboratory of Evolutionary Systematics of Vertebrates, Institute of Vertebrate Paleontology and Paleoanthropology, Chinese Academy of Sciences, Beijing, 100044, China*

https://zoobank.org/08EC18A1-ED4E-4E88-B6BB-AA44FB6810FD

Corresponding authors: Chang-Fu Zhou (zhoucf528@sdust.edu.cn); Rui Pei (peirui@ivpp.ac.cn)

Academic editor: Emanuel Tschopp ♦ **Received** 20 April 2026 ♦ **Accepted** 4 August 2026 ♦ **Published** 2 September 2026

Abstract

A new, well-preserved troodontid postcranial skeleton from the Jehol Biota of the Ningcheng Basin, Inner Mongolia, China, is described and assigned to *Sinovenator changii* based on an autapomorphy: the presence of two pneumatic foramina on the lateral surface of the anterior cervical vertebrae. This specimen is inferred to be an adult based on the presence of an external fundamental system (EFS) in the ulna, as well as the complete fusion of the cervical neural arches and centra. This represents the first record of a troodontid dinosaur from the Jehol Biota in Inner Mongolia. The discovery of this new specimen reveals additional morphological details of *Sinovenator changii* and expands the paleogeographic range of this taxon. Notably, this new specimen bears a moderately developed pubic ambiens process, in contrast to the anteroposteriorly elongated condition in Late Cretaceous troodontids. This morphology may reflect an early evolutionary phase in the elongation of the ambiens process among troodontids and might suggest a comparatively constrained hindlimb locomotor capacity relative to that of their Late Cretaceous relatives. In addition, body size comparisons among deinonychosaurians reveal that dromaeosaurids exhibit much greater size disparity than troodontids, which may reflect greater diversity in dromaeosaurid locomotion, ecological niches, or growth strategies.

Keywords

Early Cretaceous, Jehol Biota, Ningcheng Basin, postcranial skeleton, *Sinovenator*, Troodontidae

Introduction

Troodontidae is a clade of small- to medium-sized theropods, members of which are widely distributed in Cretaceous deposits across Asia and North America (Makovicky and Norell 2004). As some of the closest relatives of birds, troodontids play a crucial role in understanding the osteological transition from non-avialan dinosaurs to birds. In the last three decades, many exquisitely preserved troodontid fossils have been discovered in the Early Cretaceous Jehol Biota of northeastern China, including *Sinovenator* (Xu et al. 2002), *Sinusonasus* (Xu and Wang 2004), *Mei* (Xu and Norell 2004), *Jianianhualong* (Xu et al. 2017), *Liaoningvenator* (Shen et al. 2017a), and *Daliansaurus* (Shen et al. 2017b) from the Yixian Formation of western Liaoning; *Jinfengopteryx* (Ji et al. 2005) from the Qiaotou Formation of Hebei Province; and potentially anchiornithines from

the Tiaojishan Formation, whose phylogenetic position is still debated (Pei et al. 2017a, 2020). These discoveries have greatly improved our understanding of troodontid evolution and the evolutionary origin of birds (Xu et al. 2002, 2017; Xu and Norell 2004). Among these taxa, *Sinovenator changii*, one of the earliest-diverging troodontids (Xu et al. 2002; Pei et al. 2021), is crucial for understanding the early evolution of troodontids because it possesses both troodontid synapomorphies and paravian plesiomorphies (Xu et al. 2002; Yin et al. 2018). However, previous studies of *Sinovenator changii* have predominantly focused on the cranium (Xu et al. 2002; Yin et al. 2018; Yu et al. 2024), whereas less attention has been paid to the morphology of the postcranial skeleton. Zhang et al. (2022) reported a new dinosaurian assemblage of the Jehol Biota from Ningcheng, Chifeng, Inner Mongolia, China (Fig. 1). Three eusauropod teeth and a symmetrodont mammal (*Ningchengodon foxi*) have been reported from this site (Zhang et al. 2024a, 2024b). Most importantly, a troodontid postcranial skeleton (SDUST-V1062) was discovered in this assemblage and is described here in detail. It represents the first record of a Jehol troodontid from the Ningcheng Basin, Inner Mongolia. The discovery of this new specimen not only expands the geographic range of *Sinovenator changii* but also adds anatomical details to the postcranial osteology of this taxon.

Material and methods

SDUST-V1062 (Figs 2–14) was collected from the fossil beds at Ningcheng, Chifeng, Inner Mongolia, during field expeditions in 2014. This specimen consists of an articulated and three-dimensionally preserved postcranial skeleton, including 10 cervical vertebrae, 9 dorsal vertebrae, and 16 caudal vertebrae; multiple rib fragments; partial left and right pectoral girdles and forelimbs; a partial right pelvic girdle; and nearly complete left and right hindlimbs.

SDUST-V1062 was prepared under a Leica M165C microscope using titanium-coated steel needles. The specimen was photographed using a Nikon D750 camera. The first seven cervical vertebrae were scanned using high-resolution X-ray computed tomography (CT) at Zhejiang University with a Nikon XT H 320 device. No filters were applied during CT scanning. A total of 2,501 TIFF slices, each 40 µm thick, were generated from CT scans acquired at 90 kV and 297 µA. The 3D reconstruction was performed using VGSTUDIO MAX 3.0 (Volume Graphics, Heidelberg, Germany). Histological thin sections of SDUST-V1062 were prepared in the histology laboratory of the Key Laboratory of Vertebrate Evolution and Human Origins, IVPP. Transverse sections 30 µm thick were taken from the right ulna (Fig. 2). They were photographed under normal and cross-polarized

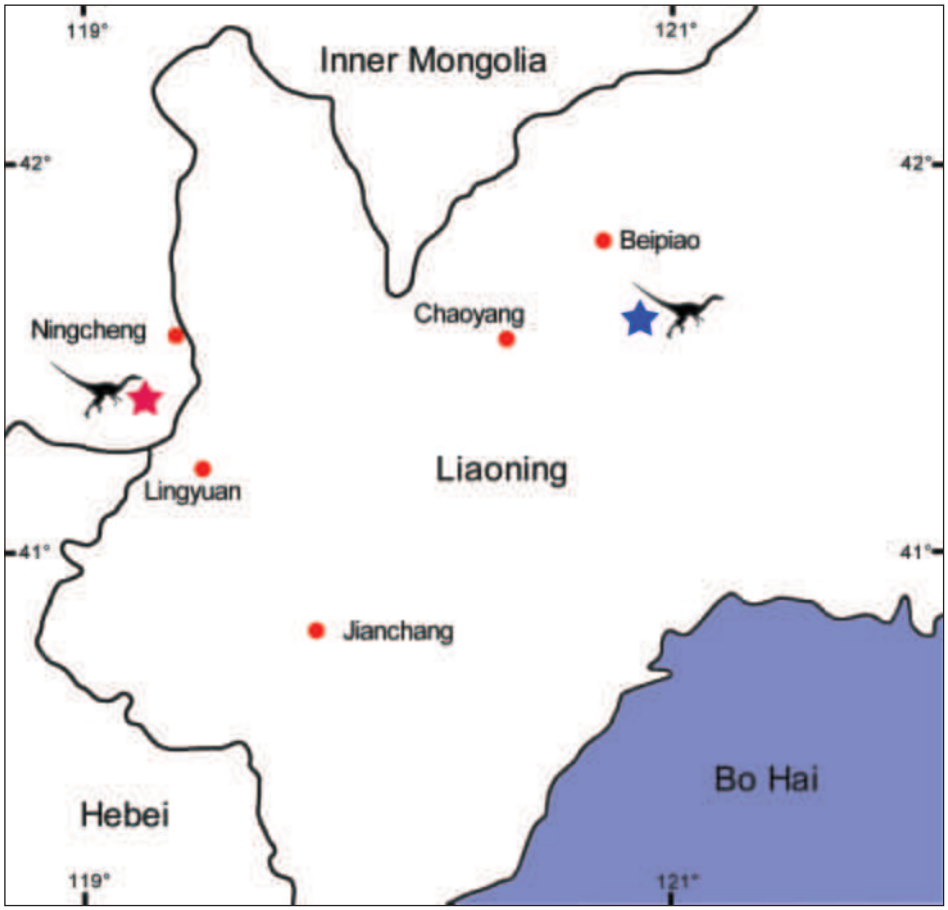

Figure 1. Area map showing the fossil locality of SDUST-V1062 in Duanjiagou, Xidayingzi, Bisiyingzi, Ningcheng, Chifeng, Inner Mongolia (red asterisk). The blue asterisk shows the main fossil-producing area of Jehol troodontids.

light using a Leica DM4 P microscope. A phylogenetic analysis was performed using TNT v. 1.5 (Goloboff et al. 2008; Goloboff and Catalano 2016). All images were processed using Photoshop CC 2018 (Adobe, California, USA). All anatomical terms for vertebral laminae and fossae follow the nomenclatural framework proposed by Wilson (1999) and Wilson et al. (2011).

Institution abbreviations

BMNHC, Beijing Museum of Natural History (Beijing, China); **DNHM**, Dalian Natural History Museum (Dalian, China); **IGM**, Mongolian Institute of Geology (Ulaan Baatar, Mongolia); **IVPP**, Institute of Vertebrate Palaeontology and Palaeoanthropology, Chinese Academy of Sciences (Beijing, China); **LH**, Long Hao Institute of Geology and Paleontology (Hohhot, China); **MOR**, Museum of the Rockies (Montana, USA); **PMOL**, Paleontological Museum of Liaoning (Shenyang, China); **SDUST**, Vertebrate Palaeontological Collection of College of Earth Science and Engineering, Shandong University of Science and Technology (Qingdao, China); **STM**, Shandong Tianyu Museum of Natural History (Linyi, China).

Systematic Paleontology

Theropoda Marsh, 1881
Maniraptora Gauthier, 1986
Troodontidae Gilmore, 1924

***Sinovenator changii* Xu et al. 2002**

Holotype. IVPP V12615, a disarticulated partial skull and partial skeleton.

Paratype. IVPP V12583, an incomplete, articulated postcranial skeleton.

Referred specimens. PMOL-AD00102, a partial skull and mandibles missing only the rostral portions, and six articulated cervical vertebrae (Yin et al. 2018); IVPP V20378, a nearly complete skeleton (Yu et al. 2024); SDUST-V1062, a nearly complete, articulated postcranial skeleton (Figs 2–14).

Locality and horizon. All reported specimens of *Sinovenator* are recovered from Lujiatun, Shangyuan, Beipiao City, western Liaoning, China. SDUST-V1062 was discovered at the Duanjiagou site, Xidayingzi Village, Bisiyingzi Township, Ningcheng County, Chifeng City, Inner Mongolia, China, a new fossil site (Fig. 1). The absolute geological age has been constrained to 125.7 ± 1.5 Ma using U–Pb zircon dating analyzed by CA-ID-IRMS (Li et al. in press), and the lithological features of the fossil beds are also the same as those of the Lujiatun Unit of the Yixian Formation at Beipiao, western Liaoning, China (Zhang et al. 2022).

Description. ***Cervical vertebrae.*** The cervical series is articulated and well exposed (Figs 2, 3). The cervicodorsal transition can be clearly distinguished by the marked length disparity between the posteriormost cervical rib and the anteriormost dorsal rib. Considering that coelurosaurs typically possess 10 cervical vertebrae (Pei et al. 2017a; Gianechini et al. 2018), it is inferred that no vertebrae are missing and that all 10 cervical vertebrae are preserved in this specimen. The proatlas and most of the cervical vertebrae are completely preserved. The eighth cervical vertebra preserves only its posterior portion (Figs 2, 3). The cervical vertebrae increase in length posteriorly, reaching their maximum length at the sixth vertebra, and then shorten posteriorly (Table 1). The neural arches and centra are completely fused.

The proatlas consists of two subtriangular, plate-like elements (Figs 2, 3). The left element taphonomically overlies the right element on its anterodorsal side. Both elements are unfused (Fig. 3), as in *Sinovenator* PMOL-AD00102 (Yin et al. 2018) and *Tsaagan* (Norell et al. 2006). The proatlas is dorsoventrally tall, similar to that in *Sinovenator* PMOL-AD00102 (Yin et al. 2018), *Tsaagan* (Norell et al. 2006), and *Archaeopteryx* (O'Connor et al. 2025), but the caudodorsal expansion present in *Archaeopteryx* is absent in SDUST-V1062. The proatlas is slightly deflected laterally. The medial surface of the proatlas is concave, as in *Sinovenator* PMOL-AD00102 (Yin et al. 2018), *Tsaagan* (Norell et al. 2006), and *Archaeopteryx* (O'Connor et al. 2025). Ventrally, the proatlas articulates with the atlantal intercentrum. Within Troodontidae, the proatlas has only been reported in *Gobivenator* (Tsuihiji et al. 2014) and *Sinovenator* (Yin et al. 2018).

The atlas comprises an intercentrum, a centrum, and two neural arches. The atlantal intercentrum is U-shaped in anterior view (Suppl. material 1), as in *Sinovenator* PMOL-AD00102 (Yin et al. 2018). The atlantal centrum, namely the odontoid, is co-ossified with the axis. The odontoid is oval and wider than tall in anterior view (Suppl. material 1). As in *Sinovenator* PMOL-AD00102 (Yin et al. 2018), the neural arch is triradiate in lateral view (Fig. 3). The postzygapophysis extends posteriorly and articulates with the axis (Fig. 3), as in *Liaoningvenator* (Shen et al. 2017a) and *Sinovenator* PMOL-AD00102 (Yin et al. 2018). No remains of atlantal ribs could be observed.

The axis is poorly preserved anteriorly. Preservation limitations preclude definitive confirmation of pneumatic foramina on the lateral surfaces of the centrum. The posterior articular facet of the centrum is slightly concave. The postzygapophysis is elongated. The epipophysis is blunt and extends posterolaterally, but not beyond the posterior margin of the postzygapophysis. This condition is similar to that of some troodontids, such as *Gobivenator* (Tsuihiji et al. 2014), *Liaoningvenator* (Shen et al. 2017a), and *Sinovenator* PMOL-AD00102 (Yin et al. 2018), and some dromaeosaurids, such as *Mahakala* (Turner et al. 2011) and *Buitreraptor* (Gianechini et al. 2018). In contrast, the epipophysis extends beyond the posterior margin of the postzygapophysis in some dromaeosaurids,

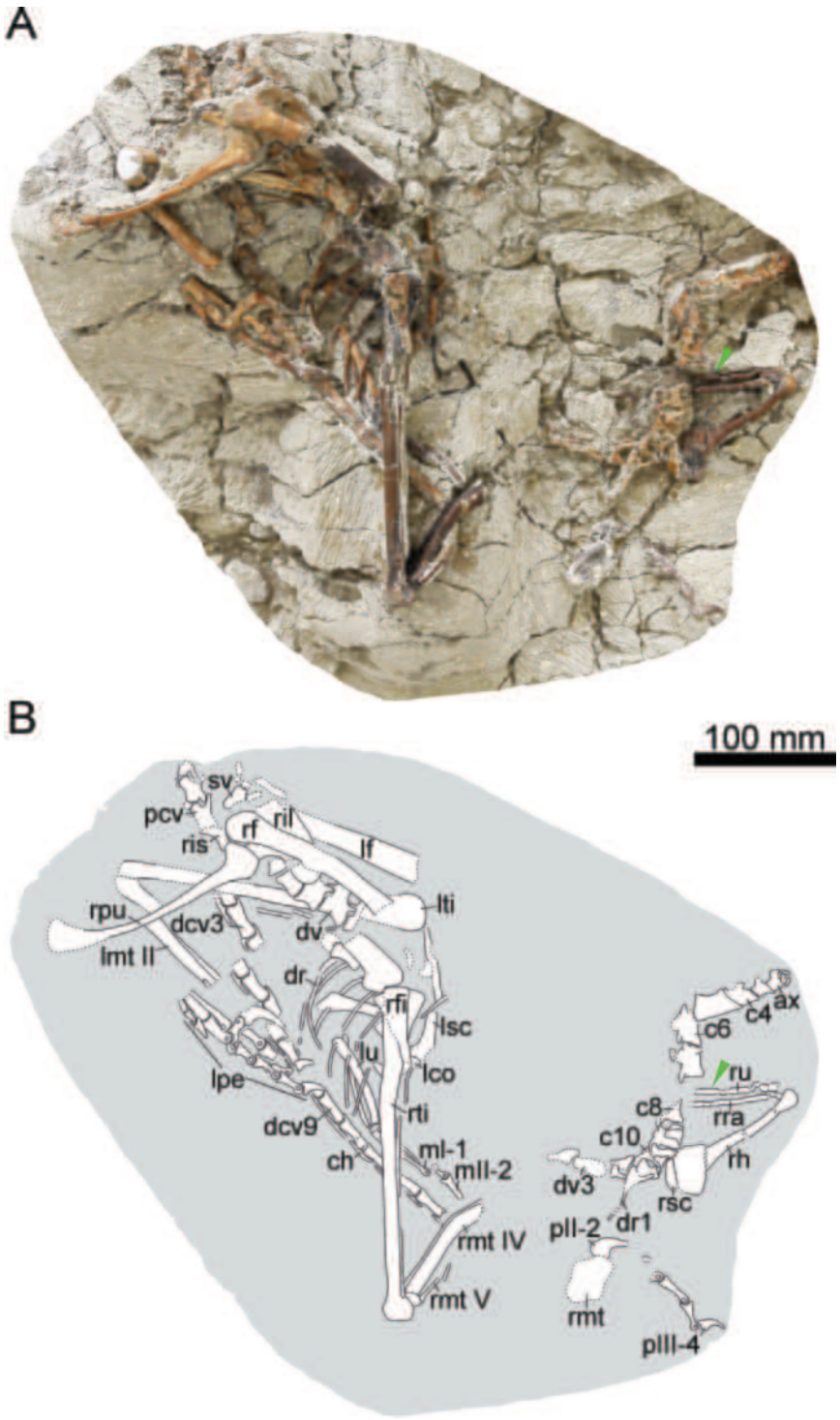

Figure 2. SDUST-V1062 in lateral view. **A.** Photograph; **B.** line drawing. The green arrow points to the sampling site for the histological thin section. Abbreviations: ax, axis; c, cervical vertebrae; ch, chevron; dcv, distal caudal vertebrae; dr, dorsal rib; dv, dorsal vertebrae; lco, left coracoid; lf, left femur; lmt, left metatarsus; lpe, left pes; lsc, left scapula; lti, left tibiotarsus; lu, left ulna; m, manual phalanx; p, pedal phalanx; pcv, proximal caudal vertebrae; rf, right femur; rfi, right fibula; rh, right humerus; ril, right ilium; ris, right ischium; rmt, right metatarsus; rpu, right pubis; rra, right radius; rsc, right scapula; rti, right tibiotarsus; ru, right ulna; sv, sacral vertebrae.

such as *Deinonychus* (Ostrom 1969) and *Tsaagan* (Norell et al. 2006). The neural spine is high and plate-like, with its posterior edge being almost vertical (Fig. 3), as in *Liaoningvenator* (Shen et al. 2017a) and *Sinovenator* PMOL-AD00102 (Yin et al. 2018). Unlike in *Gobivenator* (Tsuihiji et al. 2014) and *Jianianhualong* (Xu et al. 2017), the posterodorsal portion of the neural spine does not extend posteriorly in SDUST-V1062. The neural spine is slightly expanded bilaterally along its dorsal margin (Fig. 3). A pair of spinopostzygapophyseal laminae are well developed,

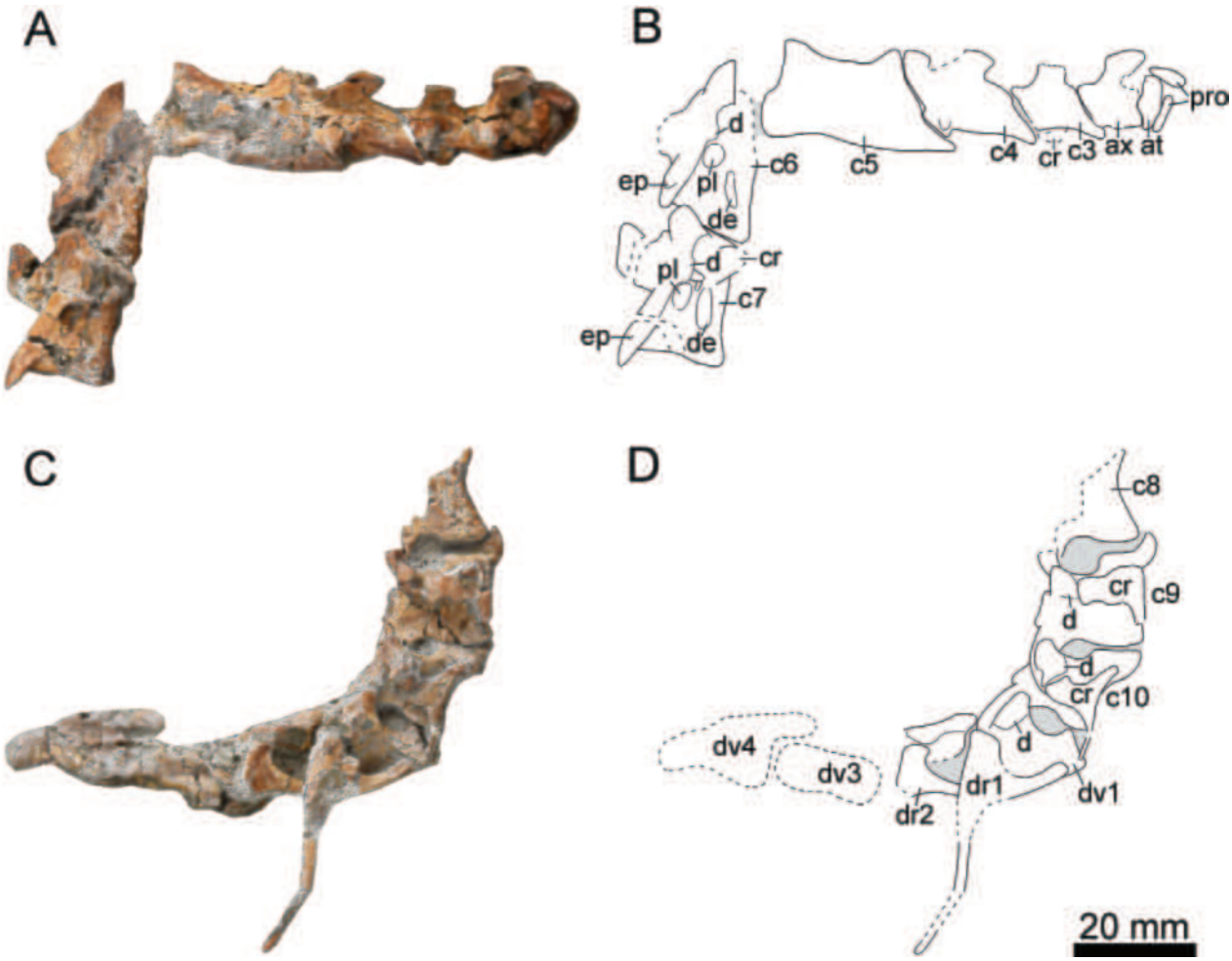

Figure 3. Cervical vertebrae and anterior dorsal vertebrae of SDUST-V1062 in lateral view. **A, C.** Photographs; **B, D.** line drawings. Abbreviations: at, atlas; ax, axis; c, cervical vertebrae; cr, cervical rib; d, diapophysis; de, depression; dr, dorsal rib; dv, dorsal vertebrae; ep, epipophysis; pl, pleurocoel; pro, proatlas.

diverge posterolaterally from the base of the neural spine, and bound the spinopostzygapophyseal fossa.

The postaxial centra are generally rectangular in lateral view (Fig. 3). The neural arches display an X-shaped profile in dorsal view. This profile is a common feature in paravians and is formed by the prezygapophyses and postzygapophyses extending anterolaterally and posterolaterally, respectively. In lateral view, the centra of the axis and the third and fourth cervical vertebrae extend posteriorly beyond the posterior margin of the neural arches (Figs 3, 4). This condition differs from that of dromaeosaurids, in which the centrum is level with or ends anterior to the posterior margin of the neural arch (Turner et al. 2012).

The third cervical vertebra is well preserved (Figs 3, 4). The ventral surface of the centrum is smooth (Fig. 4D). The lateral surface of the centrum bears two oval pneumatic foramina (pleurocoels; Currie and Dong 2001; Gao et al. 2012; Yin et al. 2018) (Fig. 4A, B), as in *Sinovenator* PMOL-AD00102 (Yin et al. 2018). These foramina are posteroventral and posterior to the diapophysis, respectively. As in *Sinovenator* PMOL-AD00102 (Yin et al. 2018), a depression is present and positioned more posteroventrally than the pneumatic foramina (Fig. 4A, B). The parapophysis is short and thick and is located at the anteroventral corner of the centrum (Fig. 4A, B). The articular facet of the parapophysis is oval and concave. The anterior articular facet of the centrum is saddle-like and transversely concave in ventral view (Fig. 4D, E), as in *Deinonychus* (Ostrom 1969) and the troodontid LH PV39 (Wang et al. 2021). The posterior articular facet of the centrum is slightly concave and posteroventrally inclined (Fig. 4F). The prezygapophysis is large, and its articular facet slopes anteroventrally and articulates with the postzygapophysis of the axis (Figs 3, 4). The epipophysis is well developed and does not extend beyond the posterior margin of the postzygapophysis (Fig. 4B), as in the axis. The diapophysis is triangular in lateral view and located on the posteroventral side of the prezygapophysis (Fig. 4A, B). The neural spine is plate-like. Dorsally, the spine is damaged but has left a subrectangular impression in the matrix (Figs 3, 4). The area of the neural spine of the third cervical vertebra is smaller than that of the axis, as in other troodontids (Tsuihiji et al. 2014; Shen et al. 2017a; Xu et al. 2017). Spinopostzygapophyseal and spinoprezygapophyseal laminae are present and diverge

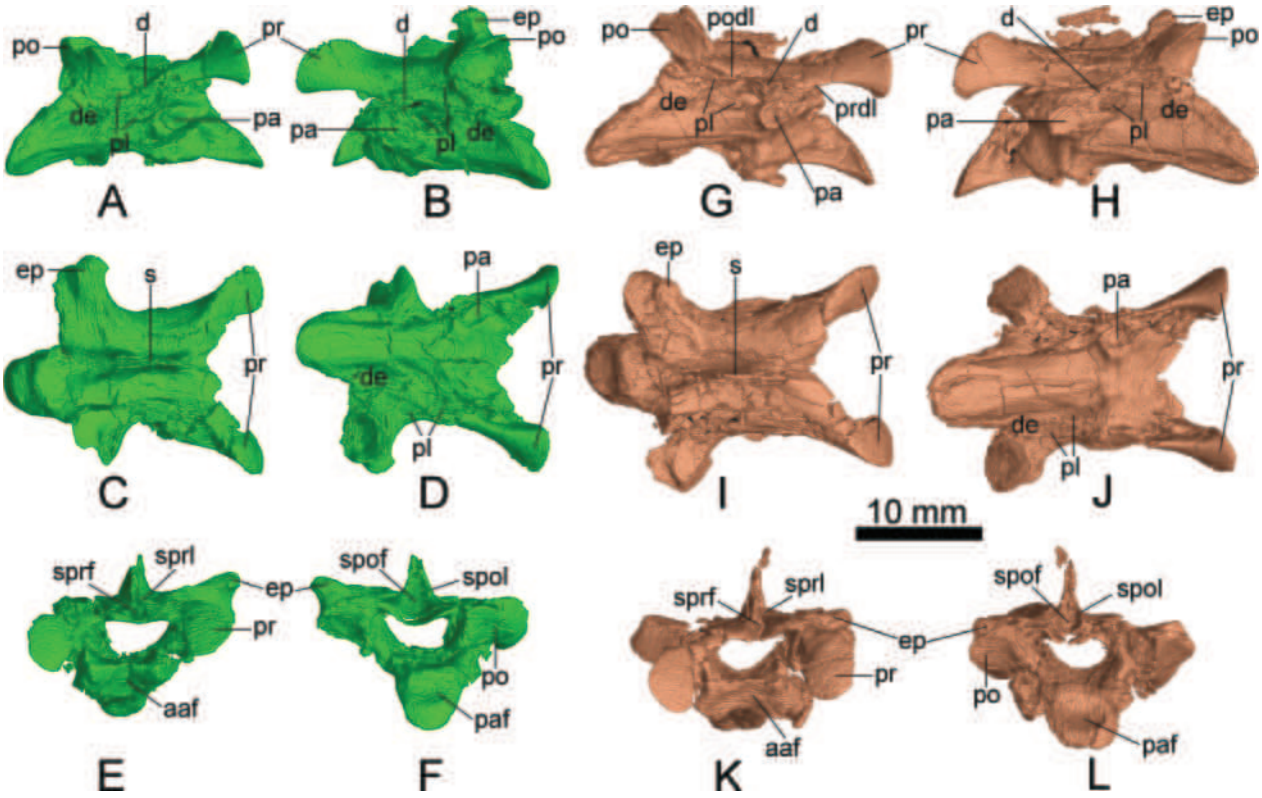

Figure 4. CT-rendered images of cervical vertebrae 3 **A–F.** and 4 **G–L.** of SDUST-V1062. **A, B, G, H.** Lateral views; **C, I.** dorsal views; **D, J.** ventral views; **E, K.** anterior views; **F, L.** posterior views. Abbreviations: aaf, anterior articular facet of the centrum; d, diapophysis; de, depression; ep, epipophysis; pa, parapophysis; paf, posterior articular facet of the centrum; pl, pleurocoel; po, postzygapophysis; podl, postzygodiapophyseal lamina; pr, prezygapophysis; prdl, prezygodiapophyseal lamina; s, neural spine; spof, spinopostzygapophyseal fossa; spol, spinopostzygapophyseal laminae; sprf, spinoprezygapophyseal fossa; sprl, spinoprezygapophyseal laminae.

posterolaterally and anterolaterally from the base of the neural spine, respectively (Fig. 4E, F). The area of the spinopostzygapophyseal fossa is larger than that of the spinoprezygapophyseal fossa (Fig. 4E, F).

The fourth cervical vertebra is well preserved (Figs 3, 4) and is clearly slightly longer than the third cervical vertebra (Table 1). Two oval pneumatic foramina and a depression occur on the lateral surface of the centrum, and their positions and morphologies are similar to those of the third cervical vertebra (Fig. 4G, H). The parapophysis is short, and its articular facet is subcircular (Fig. 4G). As in the third cervical vertebra, the anterior articular facet of the centrum is saddle-like, and the posterior articular facet is shallowly concave (Fig. 4K, L). The prezygapophysis and postzygapophysis show comparable lateral extension (Fig. 4I). The diapophysis is located on the lateral side of the neural arch and projects lateroventrally (Fig. 4G). Ventrally, the prezygapophysis bears a prezygodiapophyseal lamina that extends posteroventrally to connect with the diapophysis (Fig. 4G, H). A postzygodiapophyseal lamina is also developed between the postzygapophysis and the diapophysis. The epipophysis is slightly shorter than that of the third cervical vertebra. The neural spine is subrectangular in lateral view, and its anteroposterior length is greater than that of the third cervical vertebra. As in the third cervical vertebra, the spinopostzygapophyseal and spinoprezygapophyseal fossae are also developed (Fig. 4K, L).

The fifth cervical vertebra is poorly preserved, and its neural spine is heavily damaged (Fig. 3). This cervical vertebra is elongate and is 1.4 times the length of the fourth cervical vertebra (Table 1). The prezygapophysis is more developed than that of the fourth cervical vertebra, whereas the postzygapophysis is subequal in size to that of the fourth cervical vertebra.

The sixth cervical vertebra is the longest vertebra in the cervical series (Table 1). The anterior portion of the centrum is poorly preserved, and the parapophysis is missing (Fig. 3A, B). The ventral surface of the centrum is smooth, without the ventral keel seen in *Sinornithoides* (Russell and Dong 1993), *Troodon* (Makovicky and Norell 2004), *Saurornithoides* (Norell and Hwang 2004), and *Mei* (Gao et al. 2012; Wang et al. 2021). Posteriorly, the centrum exceeds the posterior end of the postzygapophysis (Fig. 3A, B). Owing to preservation limitations, only a suboval pneumatic foramen is visible on the lateral surface of the centrum (Fig. 3A, B). An oval depression is also present posteroventral to the pneumatic foramen (Fig. 3A, B), as in the third and fourth cervical vertebrae. The prezygapophyseal articular facet is ovoid, faces anterodorsally, and slopes slightly medially. The postzygapophysis is comparable to the prezygapophysis in size

Table 1. Selected vertebral measurements of SDUST-V1062 (mm).

Element	Value	Element	Value
Third cervical vertebra	16.0	Antepenultimate dorsal vertebra	17.0
Fourth cervical vertebra	19.9	Penultimate dorsal vertebra	16.1
Fifth cervical vertebra	28.0	Last dorsal vertebra	14.9
Sixth cervical vertebra	28.3	Penultimate proximal caudal vertebra	17.0
Seventh cervical vertebra	27.2	Last proximal caudal vertebra	19.7
Ninth cervical vertebra	24.7	Fifth distal caudal vertebra	24.2
Tenth cervical vertebra	24.6	Sixth distal caudal vertebra	26.0

For all vertebrae, the measured length extends either from the prezygapophysis to the postzygapophysis or from the prezygapophysis to the posterior articular facet of the centrum.

(Fig. 3A, B) and bears a weakly developed epipophysis dorsally. The diapophysis is located more anteriorly on the neural arch and extends laterally (Fig. 3A, B), as in *Mei* (Gao et al. 2012) and the troodontid LH PV39 (Wang et al. 2021). As in the fourth cervical vertebra, the pre- and postzygodiapophyseal laminae are also developed. The neural spine is damaged dorsally and is located between the pre- and postzygapophyses (Fig. 3A, B).

The seventh cervical vertebra is preserved in its entirety (Fig. 3A, B). This vertebra is slightly shorter than the sixth cervical vertebra. Ventrally, the centrum bears a pair of weakly developed carotid processes between the parapophyses, as in *Sinornithoides* (Currie and Dong 2001) and *Troodon* (Makovicky and Norell 2004). The shape and location of the pneumatic foramen and depression are similar to those of the sixth cervical vertebra, but the depression is slightly larger and deeper (Fig. 3A, B). The parapophysis is located at the anteroventral corner of the lateral side of the centrum and articulates with the cervical rib (Fig. 3A, B). The prezygapophysis is weakly developed and directed more dorsally than that of the sixth cervical vertebra, and the postzygapophysis extends posteriorly beyond the posterior margin of the centrum (Fig. 3A, B). The diapophysis is posterodorsal to the parapophysis. This diapophyseal location is comparable to that of the sixth cervical vertebra, but the process extends more ventrally than in the latter (Fig. 3A, B). The pre- and postzygodiapophyseal laminae are developed between the diapophysis and the pre- and postzygapophyses, respectively. The neural spine is plate-like, and its anterior margin slopes slightly anteroventrally in lateral view (Fig. 3A, B).

Only the posterior margin of the eighth cervical vertebra is preserved (Fig. 3C, D). A depression is present on the lateral surface of the centrum and is shallower than those of the preceding cervical vertebrae. The posterior articular facet of the centrum is exposed and relatively flat. The postzygapophysis extends beyond the posterior margin of the centrum.

The ninth cervical vertebra is exposed on its right side (Fig. 3C, D). In lateral view, the centrum is subrectangular and ventrally concave. The parapophysis is located on the anterior side of the centrum and articulates with the corresponding rib. The pneumatic foramen of the centrum is obscured by the associated rib. The anterior articular facet of the centrum is flat. The prezygapophysis is short, approximately half the anteroposterior length of the postzygapophysis. The diapophysis is stout and lies posterodorsal to the parapophysis (Fig. 3C, D), as in *Sinovenator* IVPP V12615 (Xu 2002) and *Liaoningvenator* (Shen et al. 2017a). The neural spine is reduced and much lower than those of the anterior cervical vertebrae (Fig. 3C, D).

The tenth cervical vertebra is subequal in length to the ninth cervical vertebra. The prezygapophysis is short, and the postzygapophysis is elongated (Fig. 3C, D). The diapophysis also lies posterodorsal to the parapophysis and extends laterally and slightly posteriorly. Its neural spine and centrum are comparable in morphology to those of the ninth cervical vertebra.

Dorsal vertebrae. The anterior four and the last five vertebrae of the dorsal series are preserved (Figs 2, 3, 5). The anterior four dorsal vertebrae articulate with the cervical series, and the third and fourth dorsal vertebrae are severely damaged (Fig. 3C, D). The last five dorsal vertebrae are exposed on the right side, and the last three dorsal vertebrae are relatively well preserved (Figs 2, 5). As in the cervical series, the neural arches are fully fused to their respective centra in the dorsal vertebrae.

The first dorsal vertebra is well exposed (Fig. 3C, D). The centrum is overlain by the first dorsal rib. The parapophysis is positioned at the anteroventral corner of the centrum, as in *Microraptor* (Hwang et al. 2002), *Gobivenator* (Tsuihiji et al. 2014), and *Buitreraptor* (Gianechini et al. 2018). Posterodorsal to the parapophysis, the diapophysis is well developed and extends posterolaterally (Fig. 3C, D). A lamina extends anteroventrally from the diapophysis to the centrum. Dorsally, the lamina borders a triangular prezygapophyseal-centrodiapophyseal fossa. As in the cervical series, the neural arch is X-shaped in dorsal view. The prezygapophysis is stout, with its articular facet directed anteromedially (Fig. 3C, D). The anteroposterior length of the postzygapophysis is approximately twice that of the prezygapophysis. The neural spine is weakly developed. Moreover, the anterior part of the second dorsal vertebra is also well exposed. Its morphology is similar to that of the first dorsal vertebra, except that the diapophysis is more developed.

The last five dorsal vertebrae are similar in morphology but decrease gradually in length. The antepenultimate dorsal vertebra is well exposed (Fig. 5). The centrum is dumbbell-shaped in lateral view (Fig. 5). Laterally, the centrum is not pneumatized. It is ventrally smooth and lacks a keel. In lateral view, the parapophysis is located anterodorsally on the centrum and projects laterally. The neural arch is formed by the anterodorsally directed prezygapophysis and the almost horizontally directed postzygapophysis (Fig. 5). Both are subequal in length. The postzygapophysis exceeds the posterior margin of the centrum. The transverse process is positioned more posteriorly on the neural arch relative to the parapophysis (Fig. 5). It is broadened and projects laterally. The neural spine is tall and rectangular in lateral view (Fig. 5).

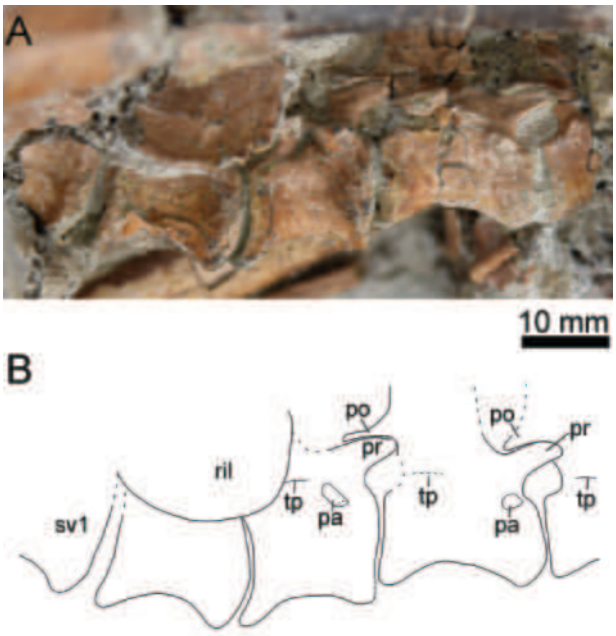

Figure 5. Posterior dorsal vertebrae of SDUST-V1062 in lateral view. **A.** Photograph; **B.** line drawing. Abbreviations: pa, parapophysis; po, postzygapophysis; pr, prezygapophysis; ril, right ilium; sv, sacral vertebrae; tp, transverse process.

Its posterior edge is apparently smooth, and the scar for attachment of the interspinous ligament is absent.

Sacral vertebrae. The sacral vertebrae are poorly preserved and partially obscured by the right ilium and femur (Fig. 2). Virtually no anatomical details can be discerned.

Caudal vertebrae. In SDUST-V1062, an incomplete segment of the caudal series is preserved in articulation (Fig. 2). Sixteen caudal vertebrae are preserved, including the last three proximal caudal vertebrae and the first 13 distal caudal vertebrae. The well-defined transition point corresponds to the caudal region where the transverse processes terminate, represents the terminus of the M. caudofemoralis attachment (Hone et al. 2021), and demarcates the proximal from the distal caudal vertebrae (Fig. 6).

Only the posterior portion of the antepenultimate proximal caudal vertebra is preserved, whereas the last two proximal caudal vertebrae are nearly complete (Fig. 6A, B). The penultimate proximal caudal vertebra is short and approximately two-thirds the length of the longest distal caudal vertebra (Table 1). In lateral view, the centrum is concave ventrally. The transverse process is poorly preserved and anteroposteriorly elongated, showing marked lateral extension (Fig. 6A, B). The pre- and postzygapophyses extend anterodorsally and posterodorsally, respectively. The postzygapophysis is short and does not extend posteriorly beyond the posterior border of the centrum (Fig. 6A, B). The last proximal caudal vertebra is slightly elongated relative to the preceding proximal caudal vertebrae. The transverse process is weakly developed, leaving a low, anteroposteriorly extended ridge (Fig. 6A, B). The postzygapophysis is shorter than the prezygapophysis and does not extend beyond the posterior margin of the centrum.

The first 13 distal caudal vertebrae are well preserved. The transverse process of the first distal caudal vertebra is absent (Fig. 6A, B). Along the series, the distal caudal vertebrae gradually elongate posteriorly, reaching their maximum length at the sixth distal caudal vertebra (Table 1). The distal caudal vertebrae are similar in morphology. In lateral view, the centra are rectangular, and the lateral surfaces bear a longitudinal depression (Fig. 6C, D). The prezygapophyses are elongated on the first six distal caudal vertebrae and then become gradually more slender and shorter posteriorly. In contrast, all postzygapophyses of the distal caudal vertebrae are strongly reduced. As in other troodontids (Makovicky and Norell 2004), the distal caudal vertebrae are sulcate along the dorsal midline, and neural spines are absent.

The anterior chevrons are poorly preserved, but the posterior chevrons are well preserved. The posterior chevrons are flattened dorsoventrally and elongated anteroposteriorly; this is a feature of derived coelurosaurians, such as dromaeosaurids, other troodontids, and basal birds (Xu 2002). These posterior chevrons are incomplete, except for the one between the tenth and eleventh distal caudal vertebrae. The anterior and posterior processes of this chevron are subequal in length (~10.5 mm; Fig. 6C, D). The anterior processes are slightly bifurcated, and the posterior processes are relatively blunt-ended in SDUST-V1062, as in *Mei* (Pei 2015), unlike in *Jianianhualong*, which has relatively blunt-ended anterior processes and slightly bifurcated posterior processes (Xu et al. 2017). Moreover, in *Sinornithoides* (Currie and Dong 2001), *Jinfengopteryx* (Ji et al. 2005), and *Gobivenator* (Pei 2015), the chevrons of the distal caudal vertebrae are bifurcated on both the anterior and posterior processes. These chevrons are separated from each other (Fig. 6C, D), as in *Mei* (Gao et al. 2012), *Gobivenator* (Tsuihiji et al. 2014), and *Jianianhualong* (Li et al. 2021), but unlike *Sinusonasus* (Xu and Wang 2004), whose chevrons contact each other and form a ventral band under the caudal centra.

Ribs. Cervical and dorsal ribs are partially preserved in SDUST-V1062 (Fig. 2). Some fragments of the cervical ribs are located near the third and seventh centra. The ninth and tenth cervical ribs are well exposed. They are double-headed, with a capitulum and tuberculum, and broad proximally (Fig. 3C, D). The capitulum of the ninth cervical rib is short and closely articulated with the centrum. The tuberculum is broad and subrectangular in lateral view. The notch separating the tuberculum from the capitulum is shallow. Distally, the rib shaft narrows. The tenth cervical rib is nearly completely preserved (Fig. 3C, D). The capitulum is elongated and tapers slightly anteriorly. The tuberculum is also subrectangular and is subequal to the capitulum in length but transversely wider than the latter (Fig. 3C, D). The notch is deeper than that of the ninth cervical rib. The shaft is slender and elongated posteriorly, exceeding the posterior margin of the tenth cervical centrum (Fig. 3C, D).

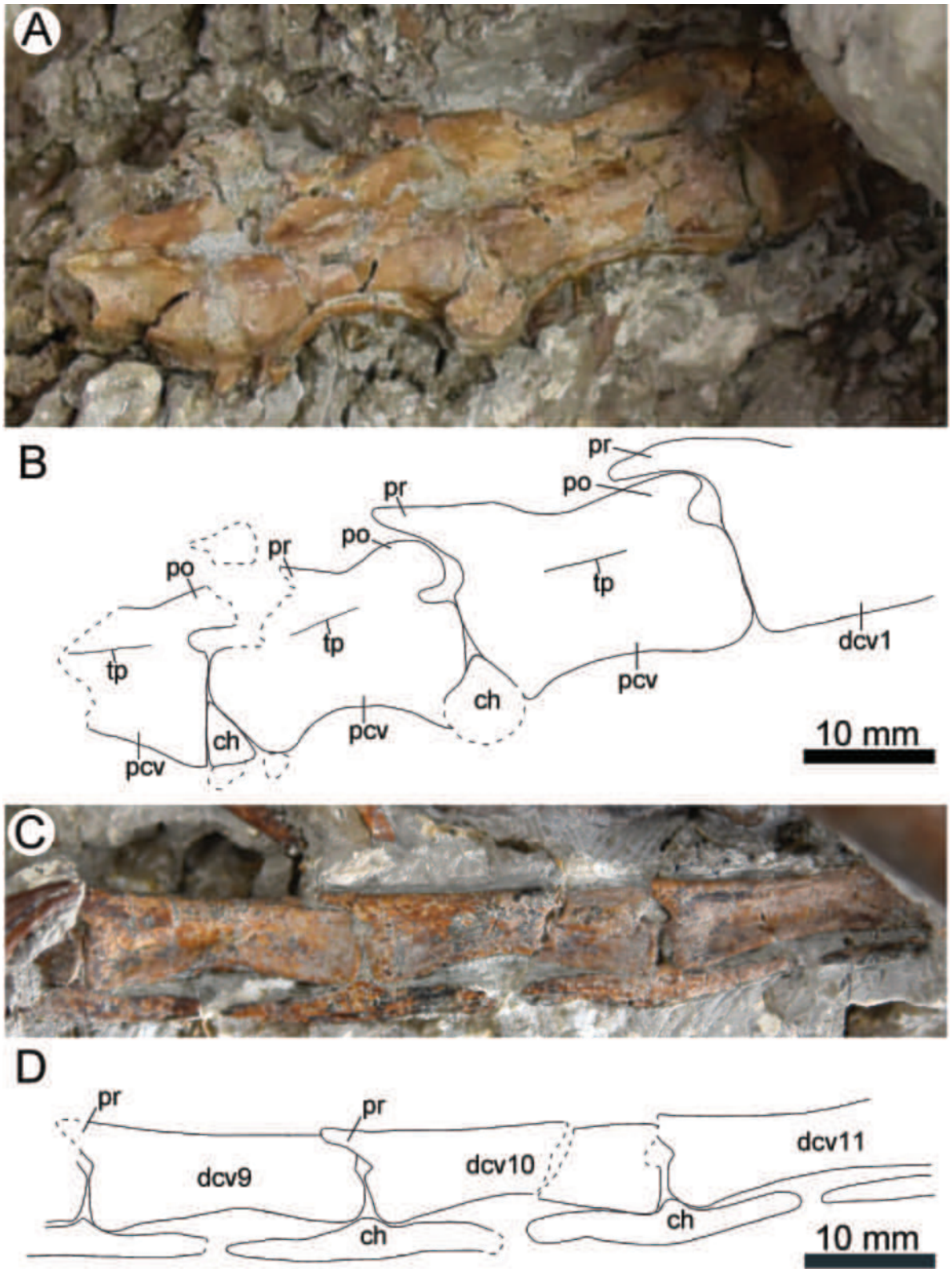

Figure 6. Caudal vertebrae of SDUST-V1062 in lateral view. **A, C.** Photographs; **B, D.** line drawings. Abbreviations: ch, chevron; dcv, distal caudal vertebrae; pcv, proximal caudal vertebrae; po, postzygapophysis; pr, prezygapophysis; tp, transverse process.

As with the cervical ribs, the first dorsal rib is also double-headed. However, the first dorsal rib is distinctly longer than the tenth cervical rib. The capitulum of the first dorsal rib is elongate, with a slightly expanded end, and the tuberculum is stout (Fig. 3C, D). The notch is deeper than those of the cervical ribs. The proximal end of the second dorsal rib is preserved. As in the first dorsal rib, the capitulum is slender and elongate, and the tuberculum is short and broad. Six other dorsal ribs are identified; they are similar in morphology, and all are extremely elongate

(Fig. 2). Their proximal ends are preserved underlying the femur, and their shafts are bowed and taper distally. As in *Archaeopteryx* (Wellnhofer 2009), *Microraptor* (Hwang et al. 2002; Pei et al. 2014), and *Anchiornis* (Pei et al. 2017a), a longitudinal groove is present along the proximal shaft of these dorsal ribs. The groove is restricted to the proximal segment of each dorsal rib, tapers distally, and exhibits natural morphology. The cross-section of the mid-shaft is elliptical. As in other troodontids (Xu et al. 2017), the uncinate processes are not preserved. No attachment scars for uncinate processes have been identified on the dorsal ribs (Fig. 2).

Pectoral girdle. The pectoral girdle of SDUST-V1062 is preserved in articulation and is composed of the scapula and coracoid (Fig. 2). The scapula and coracoid are unfused, with a distinct suture between them. The glenoid fossa is not exposed, and its orientation is unclear.

Both scapulae are exposed in SDUST-V1062 (Fig. 2). The right scapular blade is missing, and the acromion process of the left scapula is damaged. The complete scapular length was estimated based on the relatively well-preserved left scapula. The estimated length of the scapula is approximately 82% of the humeral length (Table 2). This ratio is smaller than that in other Jehol troodontids, such as *Mei* (107%, Xu and Norell 2004; 100%, Gao et al. 2012), *Jinfengopteryx* (96%; Ji et al. 2005), *Jianianhualong* (98%; Xu et al. 2017), and *Liaoningvenator* (91%; Shen et al. 2017a). The left scapula is exposed medially and is elongate and slender (Fig. 2). The scapular blade is strap-like and mediolaterally compressed. It is nearly straight in medial view, unlike the bowed shape in *Buitreraptor* (Gianechini et al. 2018). A shallow groove is present on the medial surface near the proximal end and is subparallel to the ventral margin.

The left coracoid is exposed in posterior view (Fig. 2). It is rectangular, with an extensive ventral blade, as in *Sinornithoides* (Currie and Dong 2001) and *Sinovenator* IVPP V12615 (Xu 2002). In posterior view, the coracoid is thickened dorsally and gradually thins ventrally. A circular coracoid foramen is present and located on the medioventral side of the glenoid fossa.

Forelimb. The right humerus is well preserved (Fig. 7). The humerus is 68% of the femoral length (Table 2), much like that of some troodontids, such as *Sinovenator* IVPP V12583 (68%; Xu 2002), *Jinfengopteryx* (70%; Ji et al. 2005), and *Jianianhualong* (70%; Xu et al. 2017). In contrast, the humerus is proportionally short in *Linhevenator* (approximately 40% of the femoral length; Xu et al. 2011). Proximally, the deltopectoral crest is short, making up approximately 30% of the length of the humerus (Fig. 7). This condition of a short deltopectoral crest is also present in some other troodontids, such as *Sinornithoides* (23%; Russell and Dong 1993), *Mei* (22%; Gao et al. 2012), and *Gobivenator* (30%; Tsuihiji et al. 2014), but the proportion is greater than 50% in *Linhevenator* (Xu et al. 2011). An internal tuberosity is developed and projects transversely from the proximal margin of the humerus (Fig. 7). There is no obvious groove between the humeral head and the internal tuberosity, unlike in *Liaoningvenator*, in which a groove is developed (Shen et al. 2017a). The humeral shaft is twisted approximately 90° (Fig. 7). In posterior view, a longitudinally extending, groove-like olecranon fossa is present on the distal end of the humerus (Fig. 7).

Table 2. Selected appendicular measurements of SDUST-V1062 (mm). R and L indicate right and left elements, respectively.

Element	Value	Side	Data type
Scapula	80	L	Estimated value
Coracoid	32.6	L	Measured value
Humerus	96.7	R	Measured value
Ulna	62.8	L	Measured value
Radius	62.6	L	Measured value
Metacarpal I	13.5	L	Measured value
Metacarpal II	31	L	Estimated value
Metacarpal III	31	L	Estimated value
Manual phalanx I-1	31.4	L	Measured value
Manual phalanx II-1	21.7	L	Measured value
Manual phalanx III-1	9	L	Estimated value
Manual phalanx III-2	8	L	Estimated value
Pubis	134.2	R	Measured value
Femur	143.0	R	Measured value
Tibiotarsus	205.7	R	Measured value
Fibula	190.5	R	Measured value
Metatarsal I	14.4	R	Measured value
Metatarsal II	109.6	R	Measured value
Metatarsal III	123.8	R	Measured value
Metatarsal IV	116	R	Estimated value
Pedal phalanx I-1	10.5	R	Measured value
Pedal phalanx I-2 (ungual)	11.6	R	Measured value
Pedal phalanx II-1	20.1	R	Measured value
Pedal phalanx II-2	17.7	R	Measured value
Pedal phalanx II-3 (ungual)	25	R	Estimated value
Pedal phalanx III-1	24	R	Estimated value
Pedal phalanx III-2	20.9	R	Measured value
Pedal phalanx III-3	16.7	R	Measured value
Pedal phalanx III-4 (ungual)	14.4	R	Measured value
Pedal phalanx IV-2	13.7	R	Measured value
Pedal phalanx IV-3	11.2	R	Measured value
Pedal phalanx IV-4	13.0	R	Measured value
Pedal phalanx IV-5 (ungual)	13.8	R	Measured value

Scapular length is estimated as the linear distance from the acromion process to the distal end of the scapular blade; coracoid height is measured as the dorsoventral straight-line distance; unguals are measured in a straight line from the center of the articular facet to the distal tip; all remaining elements are measured for proximodistal length.

Both ulnae and both radii are preserved (Fig. 2). The left ulna and radius are nearly complete, whereas the distal ends of the right ulna and radius are missing. The shaft of the ulna is bowed posteriorly (Fig. 2), as in many other maniraptorans (Xu 2002). In contrast, *Anchiornis* (Pei et al. 2017a) possesses a straight ulna. The cross-section of the mid-shaft is subcircular. The distal end of the ulna is transversely expanded, and its articular facet is flat.

The radius is straight (Fig. 2). It is approximately 65% of the humeral length (Table 2), whereas in *Mei* (Xu and Norell 2004), the radius is approximately 90% of the humeral length. Its mid-shaft is subcircular in cross-section and has a constant diameter. The shaft of the radius is more slender than the ulnar shaft. The diameter of the

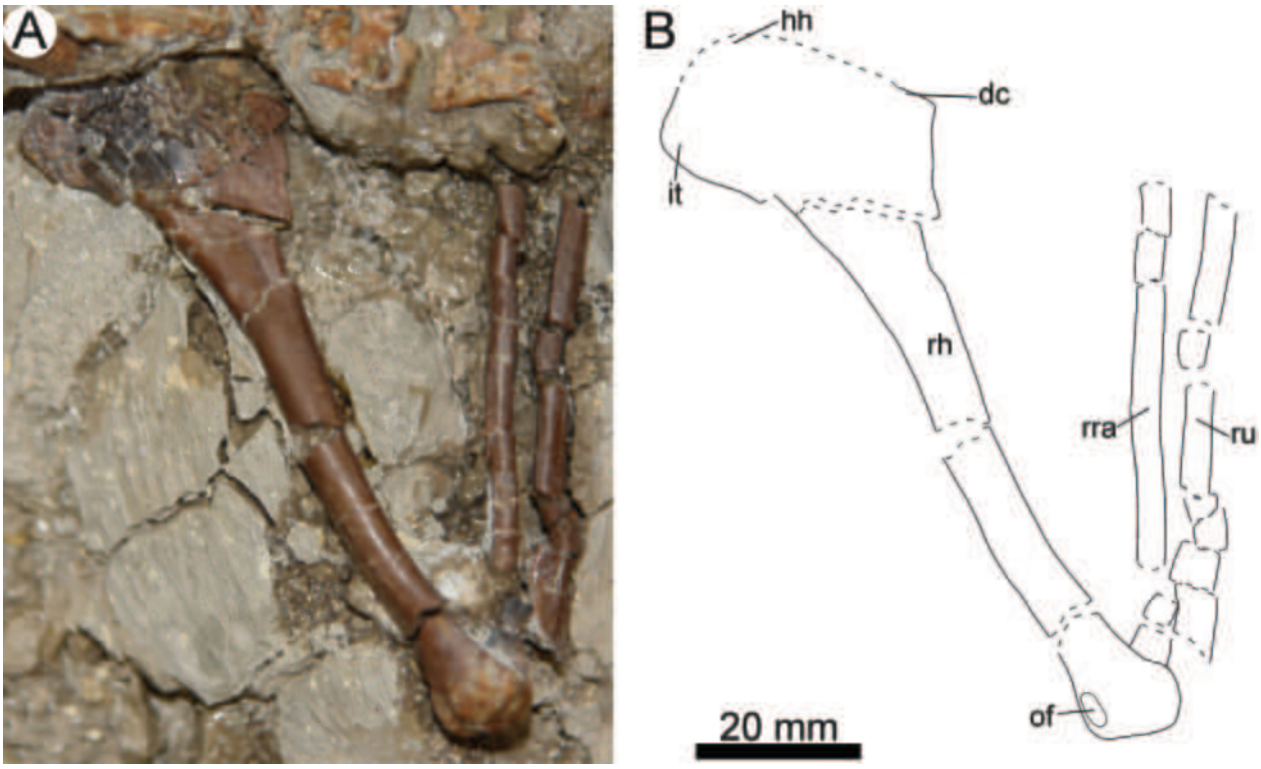

Figure 7. Right forelimb of SDUST-V1062 in posterolateral view. **A.** Photograph; **B.** line drawing. Abbreviations: dc, deltopectoral crest; hh, humeral head; it, internal tuberosity; of, olecranon fossa; rh, right humerus; rra, right radius; ru, right ulna.

mid-shaft is 2.9 mm in the left radius and approximately half that of the left ulna (5.9 mm), whereas the diameter is 3.3 mm in the right radius and only slightly less than that of the right ulna (3.8 mm), which may be an artifact of taphonomic distortion or ontogenetic variation (Figs 2, 7). Distally, the left radius is slightly curved and articulates with the radiale.

Two left carpals are preserved in SDUST-V1062: the semilunate and radiale (Fig. 2). The semilunate is larger and crescent-shaped in dorsal view, with its proximal surface being convex. Distally, it covers the proximal ends of metacarpals I and II, as in most maniraptorans (Ostrom 1969; Xu et al. 2014; Pei 2015; Napoli et al. 2025). It is closely associated with the metacarpals. The radiale is smaller and lies between the semilunate and radius.

Metacarpals I, II, and III; manual phalanges I-1, II-1, III-1, and III-2; and the proximal portion of phalanx II-2 are preserved (Figs 2, 8). Metacarpal I is the shortest of the preserved manual elements and is approximately 43% of the length of metacarpal II (Table 2). Metacarpal I is relatively robust and has a diameter of approximately 3.5 mm at the mid-shaft. Proximally, metacarpal I is closely associated with metacarpal II. The distal end of metacarpal I expands dorsoventrally and appears to be ginglymoid, as in *Mei* (Gao et al. 2012).

Metacarpals II and III are exposed in dorsal view, except that their proximal ends are obscured by the tibia (Fig. 8). They are subequal in length. The shaft of metacarpal II has a mediolateral width of approximately 2.1 mm, similar to that of metacarpal III. Metacarpal III extends distally to the level of metacarpal II (Fig. 8). However, metacarpal III extends farther distally than metacarpal II in *Mei* (Gao et al. 2012).

Manual phalanx I-1 is long and robust. The cross-section of the mid-shaft is subcircular and has a diameter of 3.3 mm, which is greater than those of metacarpals II and III (Fig. 8B, D). The combined length of manual phalanx I-1 and metacarpal I is greater than that of metacarpal II, as in *Mei* (Gao et al. 2012) and *Jianianhualong* (Xu et al. 2017). This condition differs from that of some dromaeosaurs, such as *Microraptor* (Xu et al. 2003; Pei et al. 2014), in which the combined length of phalanx I-1 and metacarpal I is shorter than that of metacarpal II. Proximally, phalanx I-1 bears a prominent ventral intercondylar tuberosity. The shaft of phalanx I-1 is slightly dorsally bowed in lateral view. The distal end is apparently ginglymoid. A collateral ligament pit is exposed on the medial surface of phalanx I-1 (Fig. 8). This ligament pit is deep and dorsally shifted on the medial face of the distal articular end. A partially preserved ungual, tentatively identified as phalanx I-2, lies on the dorsal side of the distal end of phalanx I-1, and the blood groove is visible (Fig. 8). A fragmented bony element lies isolated near the distal end of phalanx I-1, and it cannot be confidently attributed to any element of the manus (Fig. 8).

The shaft and distal end of phalanx II-1 are partially exposed (Fig. 8). The shaft is slender, with a diameter of approximately 2.3 mm. Medially, the distal end is sculptured by a deep ligament pit that is positioned centrally (Fig. 8), whereas the medial ligament pit is absent in phalanx II-1 of the unnamed troodontid SDUST-V1042 (Yu et al. 2022). Phalanx II-2 is partially preserved, and

its proximal part is well exposed. Proximally, phalanx II-2 bears well-developed ventral and dorsal intercondylar tuberosities (Fig. 8A, C), as in the unnamed troodontid SDUST-V1042 (Yu et al. 2022). The ventral tuberosity is larger than the dorsal one (Fig. 8A, C). The phalanges of digit III are comparable in diameter to those of digit II (Fig. 8B, D). Manual phalanx III-1 is subequal to phalanx III-2 in length (Table 2), as in some troodontids, such as *Jianianhualong* (Xu et al. 2017), *Hypnovenator* (Kubota et al. 2024), and the unnamed troodontids IGM 100/1126 (Pei 2015) and SDUST-V1042 (Yu et al. 2022).

Pelvic girdle. The right ilium is laterally exposed in SDUST-V1062, and the postacetabular process is missing (Fig. 9). The ilium is anteroposteriorly elongated. The preacetabular process has a convex anterior margin (Figs 5, 9), but this is possibly a taphonomic artifact. In contrast, the ilium of other troodontids, such as *Sinovenator* IVPP V12615 (Xu et al. 2002), *Mei* (Gao et al. 2012), *Jianianhualong* (Xu et al. 2017), and *Latenivenatrix* (Van der Reest and Currie 2017; Rhodes et al. 2021), has a nearly straight anterior margin. The ventral margin of the preacetabular blade slopes slightly anteroventrally, and the anteroventral process is drastically reduced (Fig. 9). The dorsal margin of the preacetabular process is roughly straight. The pubic peduncle is rectangular in lateral view and bears an articular facet that extends nearly horizontally (Fig. 9), which differs from the wedge-like pubic peduncle of *Mahakala* (Turner et al. 2011) and the unnamed troodontid IGM 100/1126 (Pei 2015). A large, deep fossa is located on the lateral surface of the pubic peduncle (Fig. 9) for the attachment of the M. cuppedicus. Dorsally, a ridge defining the fossa is well developed. It terminates dorsal to the pubic peduncle and is not continuous with the acetabular rim.

The right pubis is well preserved (Fig. 9). The pubis is nearly vertically oriented, as in *Gobivenator* (Tsuihiji et al. 2014), unlike the posteroventrally oriented condition in some basal paravians, such as *Archaeopteryx* (Ostrom 1976; O'Connor et al. 2025), *Sinornithosaurus* (Xu et al. 1999), and *Sinovenator* IVPP V12615 (Xu et al. 2002), and the anteroventrally oriented condition in *Saurornithoides* (Norell et al. 2009) and the unnamed troodontid IGM 100/1126 (Pei 2015). Proximally, the pubis projects anteriorly, forming an ambiens process (Fig. 9). The ambiens process is moderately developed, and its anteroposterior length is less than that of the ischial peduncle of the pubis, differing from the elongated condition in *Saurornithoides* (Norell et al. 2009), *Gobivenator* (Tsuihiji et al. 2014), and *Latenivenatrix* (Van der Reest and Currie 2017; Rhodes et al. 2021), in which the anteroposterior length is far greater than that of the ischial peduncle of the pubis. The pubis articulates dorsally with the pubic peduncle of the ilium along a nearly horizontal articular facet (Fig. 9). Posteriorly, the ischial peduncle of the pubis is trapezoidal in lateral view and narrows posteriorly to articulate with the ischium (Fig. 9). Distally, the pubic shaft is elongate and nearly straight but curves slightly posteriorly. It is mediolaterally flat in the proximal portion and twisted at the mid-shaft (Fig. 9). The pubic apron is transversely expanded, a characteristic of troodontids (Xu et al. 2017). The pubic apron is greater than half the length of the pubic shaft, as in *Sinovenator* IVPP V12615 (Xu 2002), but unlike in *Talos* (Zanno et al. 2011), *Gobivenator* (Tsuihiji et al. 2014), *Troodon*, and IGM 100/1126 (Pei 2015), in which the pubic apron is less than half the length of the pubis. The pubic boot is expanded posteriorly and has a slight anterior expansion (Fig. 9), as in *Gobivenator* (Tsuihiji et al. 2014) and *Almas* (Pei et al. 2017b).

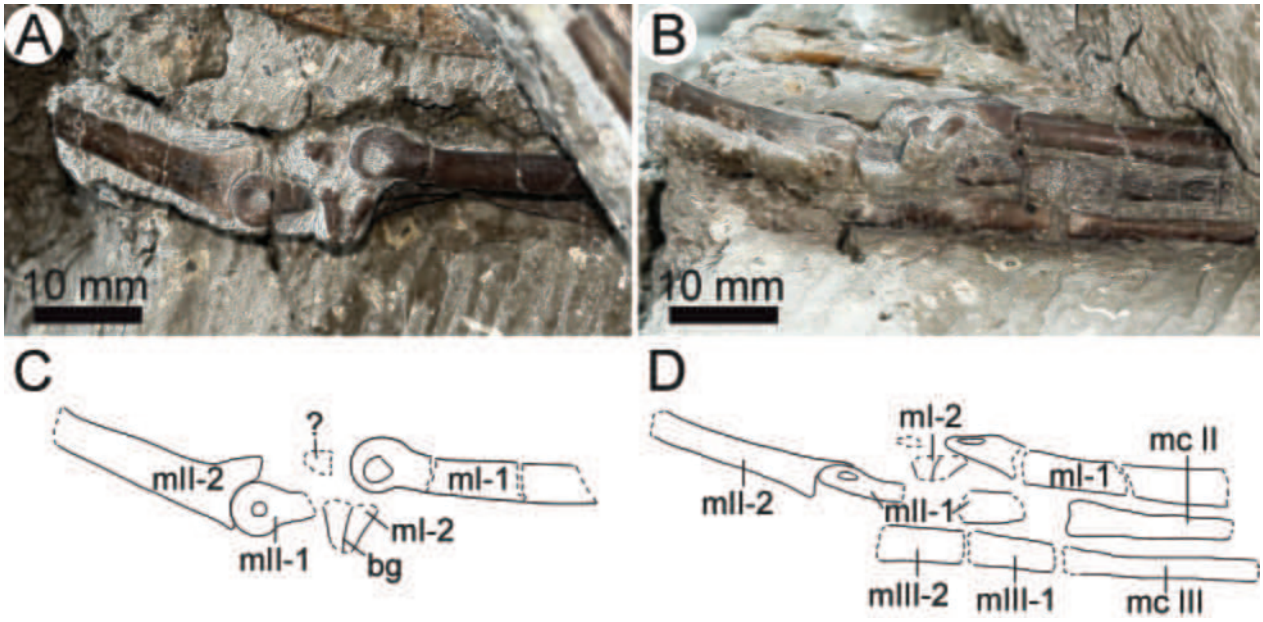

Figure 8. Left manus of SDUST-V1062 in medial view **A, C.** and dorsal view **B, D**. **A, B.** Photographs; **C, D.** line drawings. Abbreviations: bg, blood groove; m, manual phalanx; mc, metacarpal.

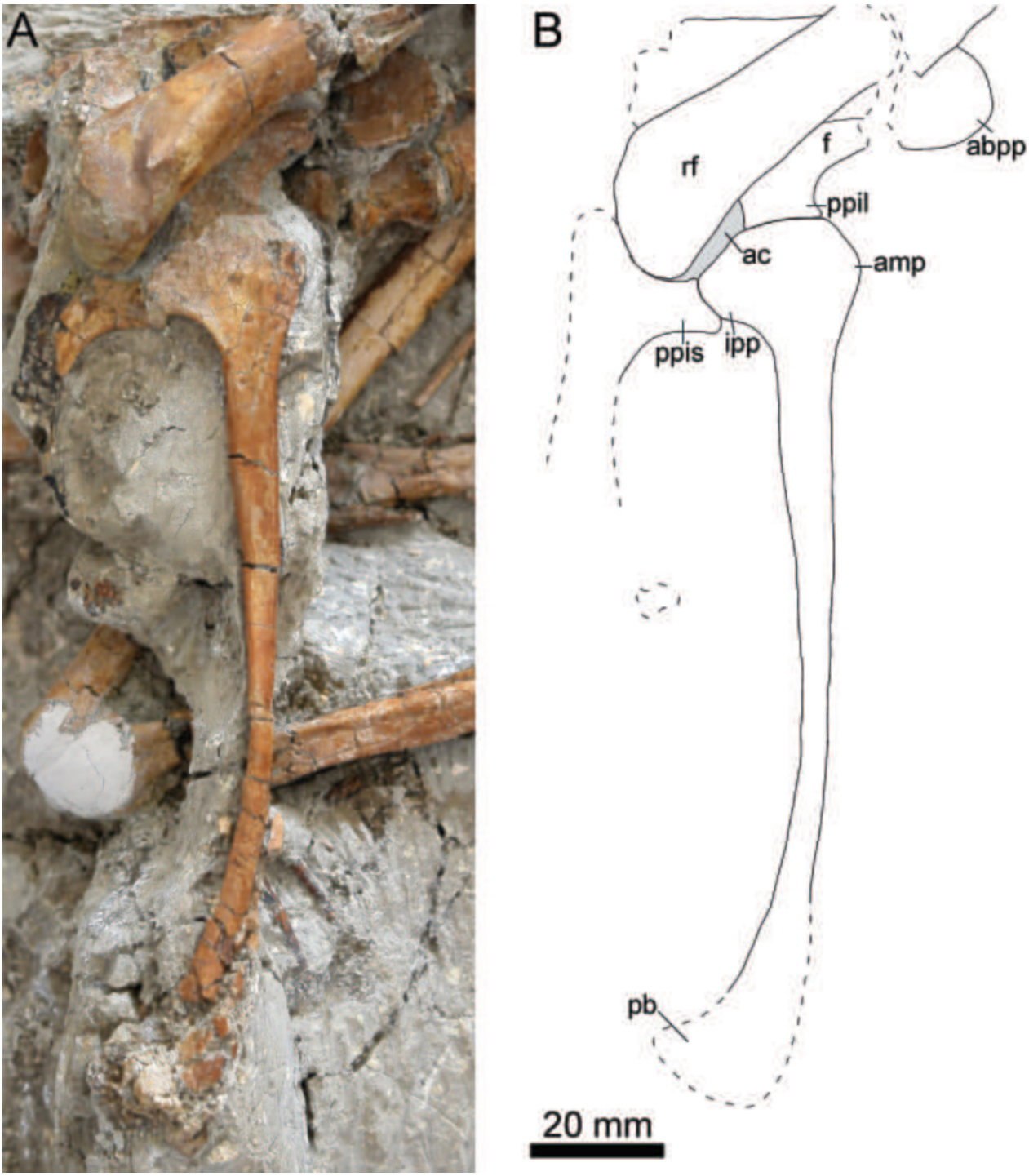

Figure 9. Pelvic girdle of SDUST-V1062 in lateral view. **A.** Photograph; **B.** line drawing. Abbreviations: abpp, anterior border of the preacetabular process; ac, acetabulum; amp, ambiens process; fo, fossa; ipp, ischial peduncle of the pubis; pb, pubic boot; ppil, pubic peduncle of the ilium; ppis, pubic peduncle of the ischium; rf, right femur.

Only the pubic peduncle of the right ischium is preserved (Fig. 9). The pubic peduncle is quadrangular in lateral view and articulates with the ischial peduncle of the pubis along an inclined articular facet.

Hindlimb. Both femora are preserved in SDUST-V1062 (Fig. 2). As in most theropods (Norell and Makovicky 1999; Xu et al. 2017), the femoral shaft is anteriorly bowed. The femoral head projects medially at approximately 90° relative to the long axis of the shaft. The greater trochanter is located on the lateral side of the femoral head (Fig. 10). Anteriorly, the proximal end of the femur is poorly preserved. Consequently, the morphology of the lesser trochanter is uncertain. The posterior trochanter lies on the posterolateral side of the femur, near the base of the greater trochanter (Fig. 10B). The posterior trochanter is developed as a large mound, as in *Sinovenator* IVPP V12615 (Xu et al. 2002) and *Gobivenator* (Tsuihiji et al. 2014), but in contrast to the

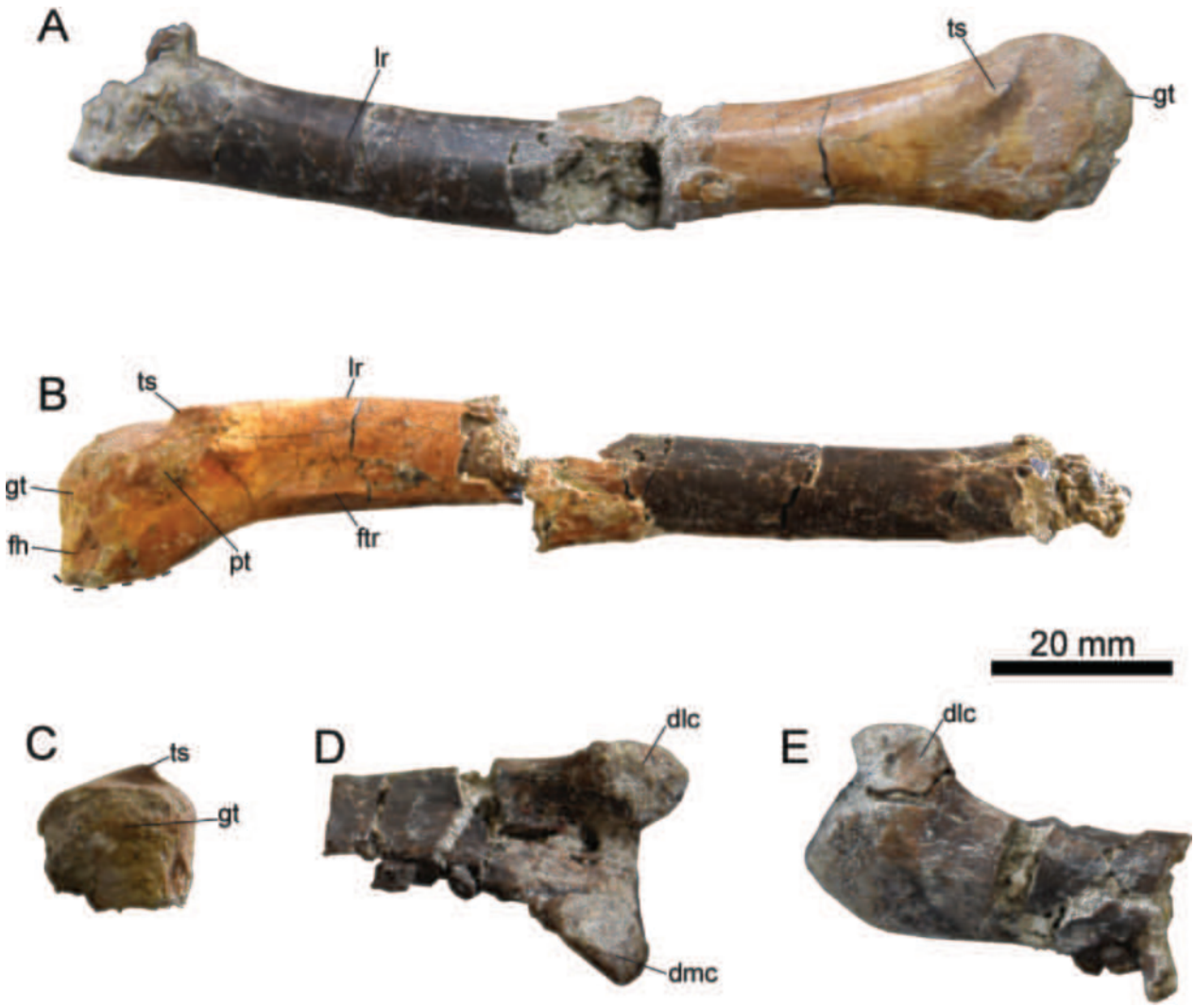

Figure 10. Right femur of SDUST-V1062. **A.** Lateral view; **B.** posterior view; **C.** proximal view; **D.** posterior view of the distal end; **E.** lateral view of the distal end. Abbreviations: dlc, distal lateral condyle; dmc, distal medial condyle; fh, femoral head; ftr, fourth trochanter; gt, greater trochanter; lr, lateral ridge; pt, posterior trochanter; ts, trochanteric shelf.

ridge-like posterior trochanter seen in *Saurornithoides* (Norell et al. 2009), *Linhevenator* (Xu et al. 2011), *Talos* (Zanno et al. 2011), and *Philovenator* (Xu et al. 2012). The trochanteric shelf is a knob-like process on the lateral surface of the proximal portion of the shaft (Fig. 10A–C). Distally, the shelf gradually becomes a low lateral ridge extending along the long axis of the femur to the lateral condyle of the distal end (Fig. 10B, E). On the posterior surface of the proximal end of the shaft, a low ridge extends longitudinally and represents a reduced fourth trochanter, the insertion position of the M. caudofemoralis longus (Fig. 10B). The cross-section of the mid-shaft is subcircular, with a diameter of 11.3 mm. Distally, the lateral and medial condyles are comparable in size (Fig. 10D). As in *Sinovenator* IVPP V12615 (Xu 2002), the lateral condyle extends more distally than the medial condyle. In posterior view, the medial condyle clearly extends medially (Fig. 10D).

Both tibiotarsi are preserved. The right tibiotarsus is well exposed, with no taphonomic deformation (Fig. 2). The tibiotarsus is long and straight (Fig. 11). It is approximately 143% of the femoral length (Table 2), similar to that of *Sinovenator* IVPP V12583 (139%), IVPP V12615 (130%; Xu et al. 2002), and *Mei* (131%; Gao et al. 2012). Proximally, as in other troodontids, the tibiotarsus is anteroposteriorly expanded, unlike the more transversely expanded element in *Sinovenator* IVPP V12583 (Xu et al. 2002). The anterior cnemial crest is well developed, expands anteriorly, and curves slightly laterally (Fig. 11B, C), a feature common to many coelurosaurs (Norell and Makovicky 1999; Makovicky et al. 2003; Gianechini et al. 2018). The lateral and posterior condyles are well developed and separated by a shallow groove (Fig. 11A). In lateral view, the lateral condyle is rounded and contacts the proximal end of the fibula. In posterior view, the lateral condyle is slightly larger than the posterior condyle. In contrast to *Sinovenator* IVPP V12583 (Xu et al. 2002), the lateral cnemial crest is absent in SDUST-V1062 (Fig. 11C). The fibular crest is present on the lateral surface and is located approximately 25.0 mm from the proximal end of the tibia, which is approximately 12% of the total tibiotarsal length.

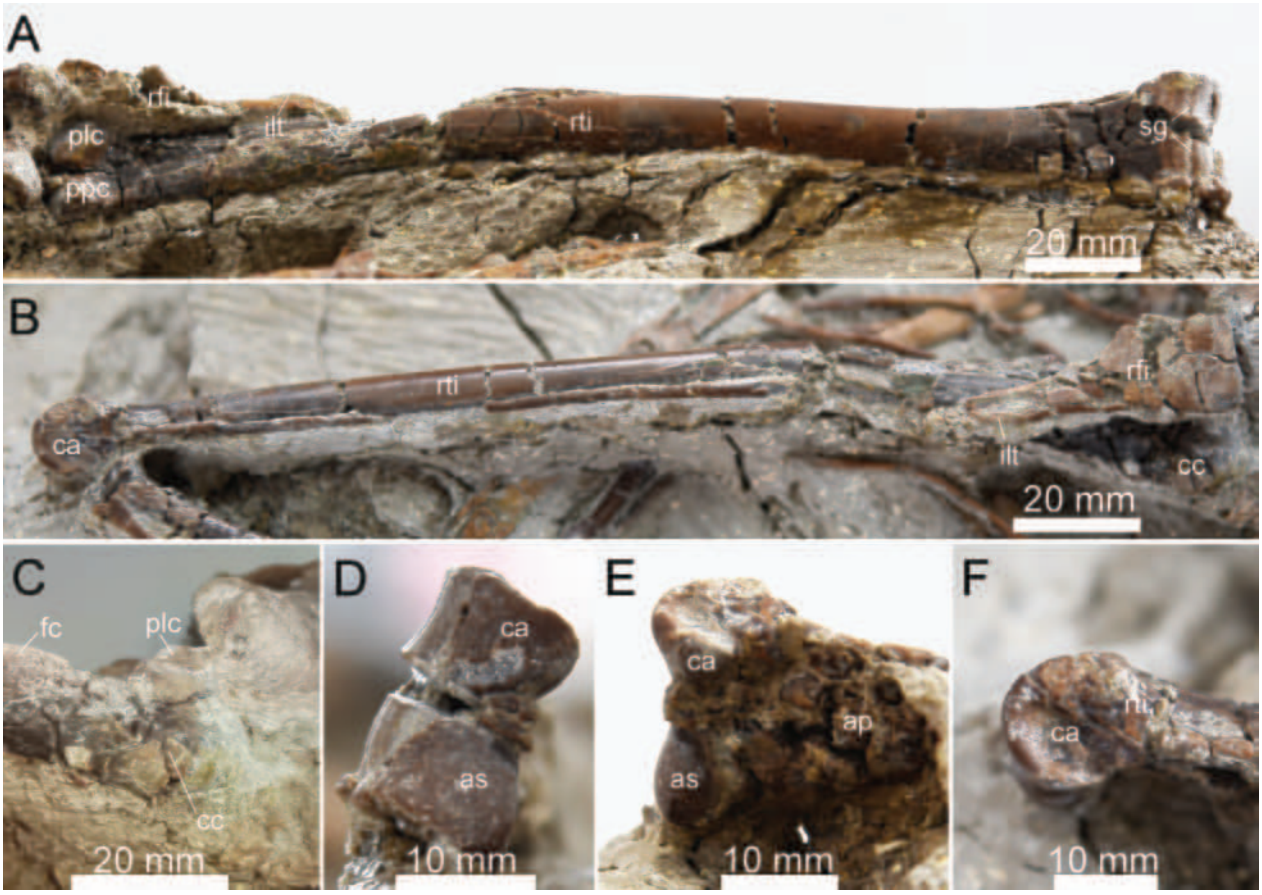

Figure 11. Right tibiotarsus and fibula of SDUST-V1062. **A.** Posterior view; **B.** lateral view; **C.** anterior view of the proximal end; **D.** distal view; **E.** anterior view of the distal end; **F.** lateral view of the distal end. Abbreviations: ap, ascending process; as, astragalus; ca, calcaneum; cc, cnemial crest; fc, fibular crest; ilt, iliofibularis tubercle; plc, proximal lateral condyle; ppc, proximal posterior condyle; rfi, right fibula; rti, right tibiotarsus; sg, shallow groove.

It is slightly deflected anteriorly, bears a sharp edge, and gradually tapers distally into the shaft. The cross-section of the mid-shaft is subcircular. Distally, the tibiotarsus expands mediolaterally. The astragalus and calcaneum are fused (Fig. 11D, E). In posterior view, a shallow groove is present between the tibia and the proximal tarsals (Fig. 11A). The ascending process of the astragalus is broken; therefore, fine anatomical features of the astragalus cannot be observed (Fig. 11E).

The right fibula is exposed, and portions of the proximal end and shaft are missing in SDUST-V1062 (Fig. 11B). The fibula is a slender element extending along the lateral edge of the tibiotarsus. Proximally, the fibula is anteroposteriorly expanded and approximately 50% of the tibial width (Fig. 11B), as in *Sinovenator* IVPP V12615 (Xu 2002). In proximal view, the articular facet of the fibula is nearly flat. An iliofibularis tubercle is developed on the lateral surface of the proximal portion of the fibula (Fig. 11A, B), approximately 30.0 mm from the proximal end of the fibula. The cross-section of the mid-shaft is subcircular, and its diameter is 2.2 mm. The distal end of the fibula articulates with the calcaneum (Fig. 11B), as in many paravians, such as *Archaeopteryx* (Ostrom 1976; O'Connor et al. 2025), *Sinornithoides* (Currie and Dong 2001), and *Microraptor* (Hwang et al. 2002).

Both tarsometatarsi are well preserved (Fig. 2). The right distal tarsals are exposed (Fig. 12). The distal tarsals cover most of the posterior portions of the proximal ends of metatarsals III and IV and overhang the metatarsus posteriorly (Fig. 12B, C). In proximal view, the proximal surface of the distal tarsals is nearly horizontal (Fig. 12C). A small notch on the posterior border of this bone possibly represents the fusion of the distal tarsals.

The left metatarsus is nearly complete but slightly compressed medially (Figs 2, 13). The right metatarsus is not deformed, but its distal end is missing (Fig. 12). Metatarsals I–IV are exposed on the left side, and metatarsals II–V are exposed on the right side. The metatarsus of SDUST-V1062 is long, approximately 123.8 mm, based on the length of metatarsal III. It is approximately 86% of the length of the femur, unlike that of *Philovenator* (125%; Xu et al. 2012). Metatarsal II is narrower mediolaterally than metatarsal IV (Fig. 12). This condition is typically asymmetrical in troodontids (Turner et al. 2012).

Metatarsal I is short and narrow (Fig. 2), as in other coelurosaurians. Metatarsal I is roughly cone-shaped and narrows proximally (Fig. 13). Distally, it forms a single condyle (Fig. 14), as in some troodontids, such as *Sinornithoides* (Currie and Dong 2001), *Talos* (Zanno et al. 2011), and *Troodon* (Fowler et al. 2011). The distal end of metatarsal I is medially offset.

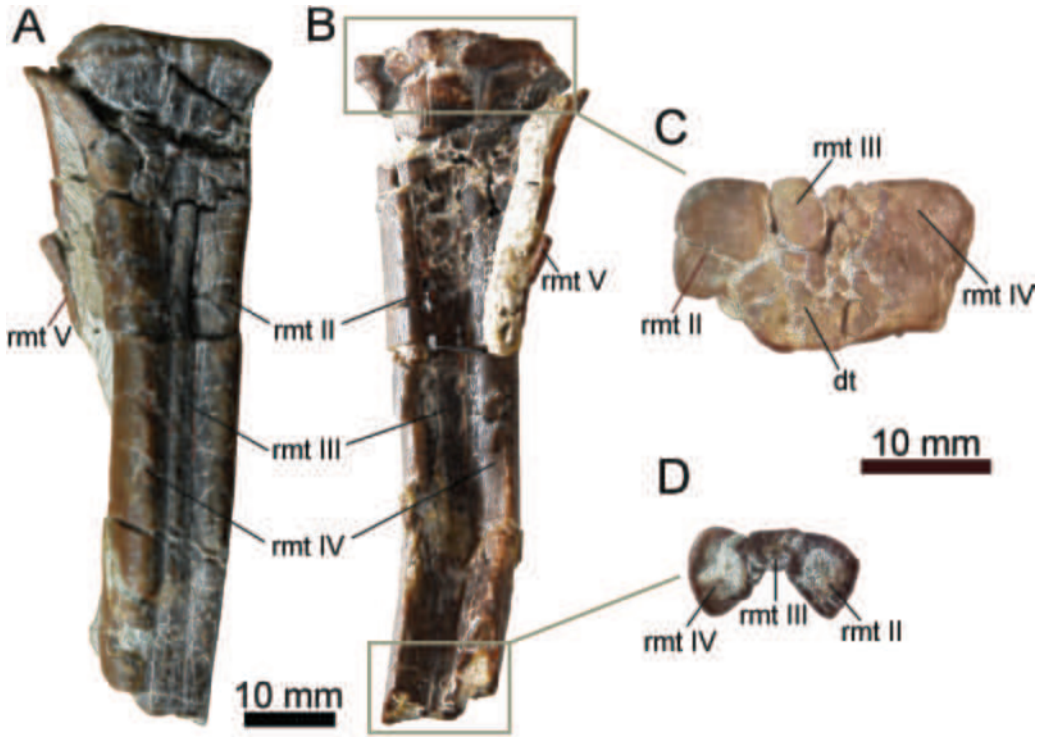

Figure 12. Right metatarsus of SDUST-V1062. **A.** Anterior view; **B.** posterior view; **C.** proximal view; **D.** cross-section of the shaft. Abbreviations: dt, distal tarsus; rmt, right metatarsus.

Metatarsal II is straight and approximately 89% of the length of metatarsal III, as in *Sinovenator* IVPP V12615 and IVPP V12583 (Xu 2002). In proximal view, the proximal end of metatarsal II is subrectangular, and its mediolateral width is approximately 8.0 mm (Fig. 12C). The mid-shaft of metatarsal II becomes subrhombic in cross-section, with a ridged posterior margin (Fig. 12B). Metatarsal II is only slightly narrower than metatarsal IV, as in *Sinovenator* IVPP V12583 (Xu et al. 2002), *Mei* (Xu and Norell 2004), and *Jinfengopteryx* (Ji et al. 2005). Distally, metatarsal II is closely associated with the medial surface of metatarsal III (Fig. 14). The distal end of metatarsal II is not ginglymoid, as in other troodontids (Xu et al. 2017). In medial view, the ligament pit is absent from the distal end (Fig. 14).

Metatarsal III is constricted between metatarsals II and IV. The proximal end of metatarsal III is not strongly constricted and is visible in anterior view (Fig. 12A), representing a subarctometatarsalian condition, as in *Sinovenator* IVPP V12583 (Xu et al. 2002), *Mei* (Xu and Norell 2004), and some dromaeosaurids, such as *Sinornithosaurus* (Xu et al. 1999) and *Microraptor* (Turner et al. 2012). Proximally, metatarsal III extends anteriorly to the same plane as metatarsals II and IV (Fig. 12A, C). In proximal view, the mediolateral width of metatarsal III is approximately 4.5 mm. The cross-section of the mid-shaft is subrectangular, and its mediolateral width is approximately 4.0 mm in anterior view. In posterior view, the shaft of metatarsal III does not extend posteriorly to the same plane as metatarsals II and IV (Figs 12, 13). Distally, metatarsal III extends beyond metatarsals II and IV, as in most troodontids, but in *Tochisaurus* (Kurzanov and Osmólska 1991) and *Talos* (Zanno et al. 2011), the distal end of metatarsal III is almost level with that of metatarsal IV. At the distal end of metatarsal III, a distinct extensor fossa is developed on the anterior surface (Fig. 14). A lateral bony tab proximal to the distal condyles is absent, as in *Sinovenator* IVPP V12583 (Xu et al. 2002) and *Saurornithoides* (Norell et al. 2009), whereas the tab is developed in the unnamed troodontid IGM 100/44 (Barsbold et al. 1987) and *Talos* (Zanno et al. 2011). A subcircular ligament pit is present on the medial side of the distal end (Fig. 14).

Metatarsal IV is the most robust element of the metatarsus (Fig. 12A, B), as in other troodontids (Xu et al. 2017). It is longer than metatarsal II but shorter than metatarsal III. In proximal view, metatarsal IV is mediolaterally widened (Fig. 12C). The anterior surface is flattened proximally and gradually becomes ridged distally (Fig. 12A). A flange is present posteriorly on metatarsal IV (Fig. 12B), as in most deinonychosaurians. The mid-shaft of metatarsal IV is subtriangular in cross-section. In posterior view, the shafts of metatarsals IV and II are nearly parallel and do not contact each other (Fig. 12B), unlike the condition in *Mei* (Xu and Norell 2004) and Late Cretaceous troodontids, such as *Tochisaurus* (Kurzanov and Osmólska 1991), *Philovenator* (Xu et al. 2012), and IGM 100/1126 (Pei 2015). The distal end of metatarsal IV reaches the level of the ligament pit of metatarsal III, as in

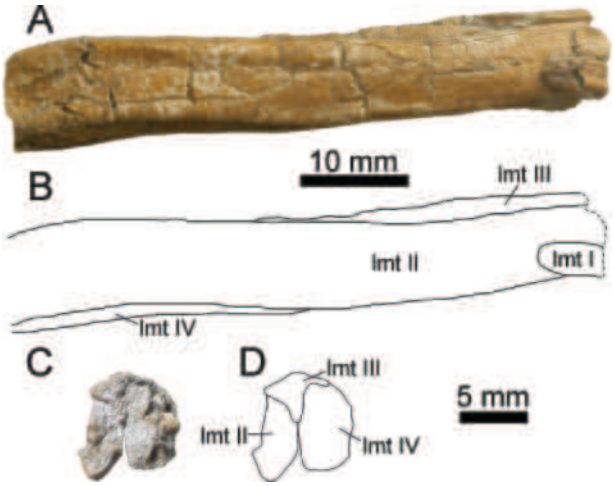

Figure 13. Left metatarsus of SDUST-V1062 in medial view **A, B.** and cross-section **C, D**. **A, C.** Photographs; **B, D.** line drawings. Abbreviations: lmt, left metatarsus.

Sinovenator IVPP V12583 (Xu et al. 2002) and *Mei* (Xu and Norell 2004).

The right metatarsal V is missing its distal margin (Fig. 12A, B). The preserved portion is a very slender bone. Proximally, metatarsal V is slightly expanded transversely and closely attached to the lateral surface of metatarsal IV (Fig. 12A, B). Distally, metatarsal V narrows gradually. It is oval in cross-section and mediolaterally wider than anteroposteriorly tall.

All digits of the left pes are well preserved (Figs 2, 14). In contrast, the right pes preserves only part of pedal digit III. As in other coelurosaurians (Makovicky and Norell 2004), the pedal phalangeal formula is 2-3-4-5-0 in SDUST-V1062.

Pedal digit I is short and does not extend beyond the distal end of metatarsal III (Fig. 14), in contrast to *Mei* (Xu and Norell 2004) and *Jianianhualong* (Xu et al. 2017). Phalanx I-1 is slender and is the shortest phalanx (Table 2). The distal end of phalanx I-1 is ginglymoid (Fig. 14). Pedal ungual I is smaller than the other pedal unguals. The flexor tubercle is weakly developed. The blood groove is weakly developed and positioned relatively ventrally on the medial surface (Fig. 14).

Pedal digit II is more robust than the other pedal digits (Fig. 14). Phalanx II-2 is approximately 88% of the length of phalanx II-1 (Table 2). This ratio is larger than that in some early-diverging troodontids, such as *Sinovenator* IVPP V12615 (67%) and *Jianianhualong* (69%), indicating a relatively unreduced phalanx II-2. The distal end of phalanx II-1 is ginglymoid, with two asymmetrical condyles, and the lateral condyle is larger than the medial condyle. A circular ligament pit is exposed on the medial surface of the distal end of phalanx II-1 and is positioned near the center of the distal portion of the phalanx (Fig. 14). Phalanx II-2 bears a prominent ventral intercondylar tuberosity (Fig. 14), as in other deinonychosaurians (Turner et al. 2012; Xu et al. 2017). The shaft of phalanx II-2 is slightly constricted at its midlength, and its dorsoventral height is approximately 5.4 mm. The distal end of phalanx II-2 is subcircular in medial view, and the ligament pit is oval (Fig. 14). Pedal ungual II is damaged at the proximodorsal portion and distal tip. It is larger than the other unguals and strongly curved (Fig. 14), as in other deinonychosaurians (Turner et al. 2012). A flexor tubercle is strongly developed, implying the presence of flexor muscles (Ostrom 1969). The blood groove is distinct and tapers distally (Fig. 14).

Pedal digit III is the longest digit of the pes (Fig. 14). Phalanx III-1 is partially exposed. The ligament pit is well developed, circular, and centrally positioned on the medial surface of the distal end (Fig. 14). Proximally, the dorsoventral height of phalanx III-2 is 8.6 mm and gradually decreases distally. The distal articular end of phalanx III-2 is ginglymoid. The ligament pit is large and oval and is located in the center of the medial surface of the distal end (Fig. 14). Phalanx III-3 is shorter than phalanx III-2. The ligament pit is oval and dorsally shifted on the medial surface of the distal end (Fig. 14). Pedal ungual III is significantly smaller and less curved than pedal ungual II, as in other troodontids (Turner et al. 2012). The flexor tubercle is weakly developed, and the blood groove is positioned relatively ventrally along the medial surface. The proximodorsal lip, a raised bony flange, is developed (Fig. 14), as in *Hypnovenator* (Kubota et al. 2024).

Pedal digit IV includes five phalanges, and phalanx IV-1 is covered by digit II. Phalanges IV-2, IV-3, and IV-4 are similar in morphology, and the ligament pits are well developed at their distal ends (Fig. 14). The distal end of phalanx IV-4 is ginglymoid, with two symmetrical condyles. Pedal ungual IV is slightly larger than ungual I but smaller than ungual III (Fig. 14). The morphologies of the flexor tubercle and blood groove are similar to those of ungual III.

Phylogenetic analyses

To determine the phylogenetic position of SDUST-V1062, the data matrix for coelurosaurians published by Pei et al. (2020, 2021) was used, with SDUST-V1062 added (170 taxa and 853 characters). The phylogenetic matrix and tree files are deposited in and publicly accessible through MorphoBank. A total of 140 characters were treated as ordered, whereas all remaining characters were treated as unordered. Polymorphic character scoring was implemented throughout the matrix. Taxa exhibiting multiple morphological states for a single character were coded with combined-state notations (e.g., [0 1]) directly within the matrix instead of using the any-instance, missing-data, or three-state scaled coding schemes. The operational taxonomic unit (OTU) of *Sinovenator* was scored based on the holotype IVPP V12615 and paratype IVPP V12583.

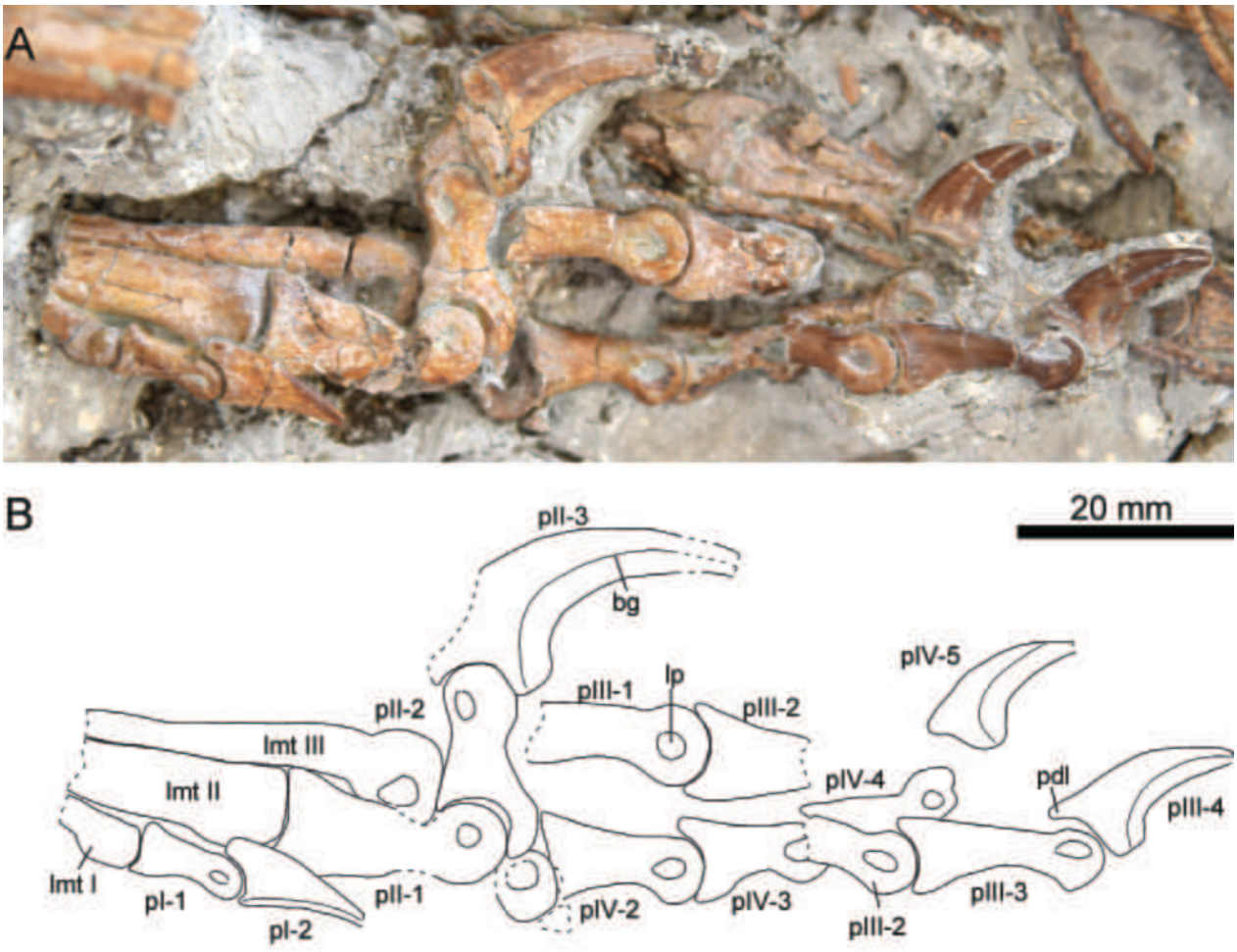

Figure 14. Left pedal digits of SDUST-V1062 in medial view. **A.** Photograph; **B.** line drawing. Abbreviations: bg, blood groove; lmt, left metatarsus; lp, ligament pit; p, pedal phalanx; pdl, proximodorsal lip.

To cross-validate the results and improve the reliability of the inferences, separate phylogenetic parsimony analyses under equal weighting and implied weighting were performed on the character matrix. Both analyses were conducted using the "traditional search" in TNT version 1.5 (Goloboff et al. 2008; Goloboff and Catalano 2016). The maximum number of trees held in memory was set to 50,000. The traditional search strategy used 1,000 replicates of Wagner trees, TBR branch swapping, and 10 trees held per replicate.

The analysis under equal weighting produced 50 most parsimonious trees (MPTs), with a length of 3,509 steps, CI = 0.309, and RI = 0.780. In the strict consensus tree, SDUST-V1062, *Jinfengopteryx*, *Mei*, and *Sinovenator* are recovered as a clade forming the earliest-diverging branch within Troodontidae, and SDUST-V1062 is recovered as the sister group of *Sinovenator* (Fig. 15A). *Jianianhualong*, IGM 100/44, *Sinornithoides*, and *Sinusonasus* are recovered as a paraphyletic assemblage. All Late Cretaceous troodontids are recovered as a monophyletic group, and *Almas* is recovered as the earliest-diverging taxon of this clade, as in previous studies (Pei et al. 2017b, 2021).

To improve the topological resolution of the strict consensus tree obtained under equal weighting, the agreement subtree was also calculated (Tschopp and Upchurch 2018) (Fig. 15B). The agreement subtree routine implemented in TNT automatically pruned 27 phylogenetically unstable terminal taxa. Within Troodontidae, IGM 100/44 and *Byronosaurus* were among the pruned unstable terminals. In the agreement subtree, SDUST-V1062 is also recovered as the sister group of *Sinovenator* (Fig. 15B). *Jianianhualong*, *Sinornithoides*, and *Sinusonasus* exhibit well-resolved topological relationships. The topological relationships among the Late Cretaceous troodontids remain unchanged.

The analysis under implied weighting ($k = 15$; Ezcurra 2024) produced 790 MPTs, with a length of 3,514 steps, CI = 0.308, and RI = 0.780. The topological relationships within Troodontidae in the strict consensus tree derived from implied weighting are identical to those recovered under equal weighting. SDUST-V1062 is again recovered as the sister group of *Sinovenator*. Although the strict consensus trees from implied weighting and equal weighting show topological discrepancies for other

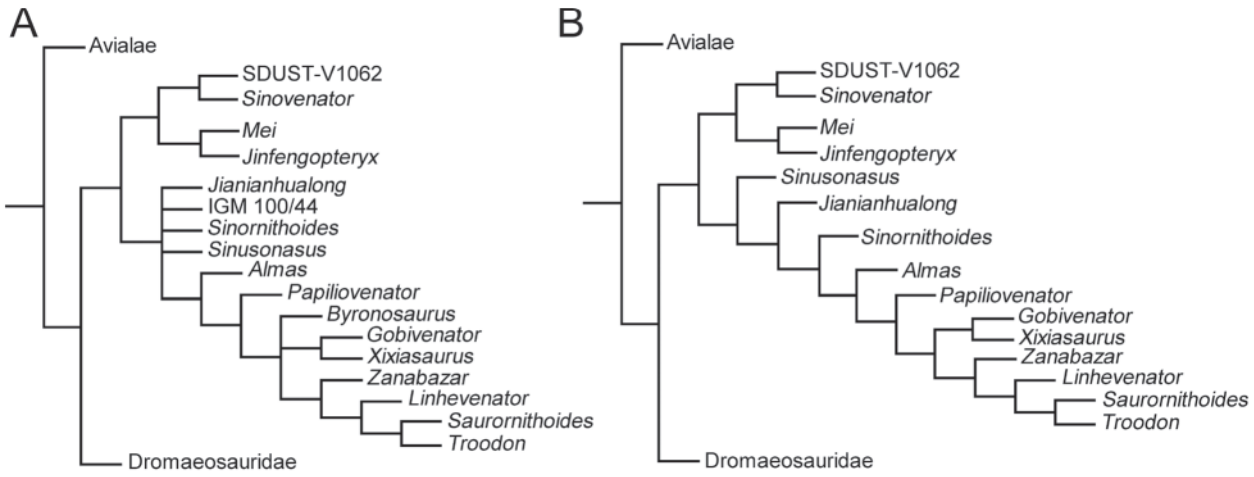

Figure 15. Phylogenetic reconstruction. Reduced topologies based on **A.** the strict consensus tree and **B.** the agreement subtree under equal weighting.

clades, these differences lie beyond the primary focus of this study. Consistent with the strict consensus tree, the agreement subtree calculated under implied weighting recovers troodontid topological relationships identical to those from the equal-weighting analyses. Full topologies of the strict consensus trees and agreement subtrees recovered under equal weighting and implied weighting are provided in Suppl. material 2.

Osteohistological study

An osteohistological analysis was conducted to further determine the ontogenetic stage of SDUST-V1062. Osteohistological samples were taken from the right ulna at a fracture approximately 40.0 mm distal to its proximal end (Fig. 2).

The thin section of the ulna has an elliptical shape, with the major axis measuring approximately 4.3 mm and the minor axis measuring approximately 3.6 mm (Fig. 16). The medullary cavity is large (2.8 mm × 2.1 mm). A distinct, thin internal circumferential layer of bone (endosteal lamellar bone, approximately 0.1 mm thick) is present, indicating that the expansion of the medullary cavity was nearly complete (Shen et al. 2017c; Pei et al. 2021). The cortex of the bone is primarily formed by fibrolamellar bone, with predominantly longitudinal vascular canals (Fig. 16A, B). The density of vascular canals and osteocytes decreases from the inner to the outer cortex (Fig. 16A, B). Secondary osteons (Haversian systems) are present in the inner cortex (Fig. 16C, D). Four lines of arrested growth (LAGs) are observed (Fig. 16C). The spacing among the outer three LAGs is extremely narrow, and this area is nearly avascular. This avascular area is interpreted here as the external fundamental system (EFS) (Fig. 16A, C). All osteohistological evidence indicates that SDUST-V1062 had almost attained its maximum somatic size when the individual died.

Discussion

Taxonomic identification of SDUST-V1062 and comparisons with other Jehol troodontids

SDUST-V1062 can be referred to Troodontidae based on the combination of the following characters: the neural spines of the distal caudal vertebrae are absent, and the remaining midline sulci are centered on the neural arches; the presence of an asymmetrical foot with a slender metatarsal II and robust metatarsal IV; the distal end of metatarsal II is not ginglymoid; and manual phalanges III-1 and III-2 are subequal in length. These features are regarded as synapomorphies of Troodontidae in different studies (Makovicky and Norell 2004; Turner et al. 2012). Within Troodontidae, SDUST-V1062 shows affinity with early-diverging troodontids and differs from late-diverging troodontids based on the presence of a subarctometatarsalian pes and a slightly asymmetrical metatarsus, with metatarsal IV being slightly wider mediolaterally than metatarsal II.

SDUST-V1062 is assigned to *Sinovenator changii* in this study based on the presence of two pneumatic foramina on the lateral surface of the anterior cervical vertebrae (Fig. 4A, B, G, H), a diagnostic feature of *Sinovenator changii* (Yin et al. 2018). The phylogenetic analyses recovered SDUST-V1062 as the sister group of *Sinovenator*, which further supports this view. In the holotype of *Sinovenator changii* (IVPP V12615), a possible anterior cervical vertebra has been identified, and two similar pneumatic foramina are also developed (Xu 2002: fig. 39A). In contrast, another postcranial diagnostic feature of *Sinovenator changii* reported in IVPP V12583—a prominent lateral cnemial crest continuous with the fibular crest at the proximal end of the tibia—is absent in SDUST-V1062 (Xu et al. 2002; Yin et al. 2018) (Fig. 11C). Notably, the proximal tibial morphology of the referred specimen of *Sinovenator changii* (IVPP V12583) is possibly unusual: the proximal

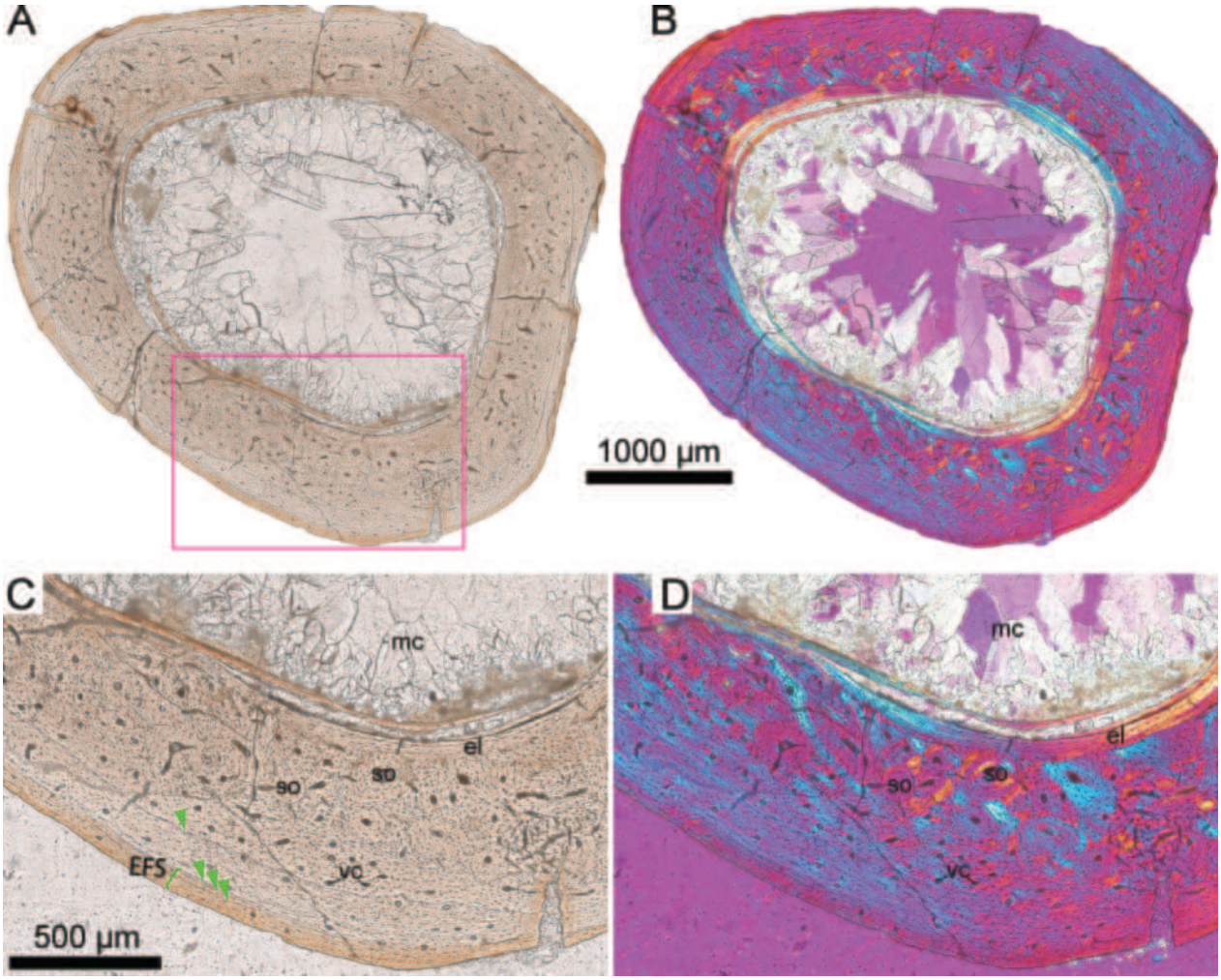

Figure 16. Histological thin section of the right ulna of SDUST-V1062 (30 µm thick). Whole cross-section **A, B.** and enlarged image **C, D.** under plain and cross-polarized light. Green arrows point to LAGs. Abbreviations: EFS, external fundamental system; el, endosteal lamella; mc, medullary cavity; so, secondary osteon; vc, vascular canal.

tibia is transversely expanded, in contrast to the anteroposteriorly elongated condition present in SDUST-V1062 and other troodontids. Moreover, IVPP V12583 is relatively poorly preserved, which suggests that its proximal tibial morphology may have been affected by taphonomic processes. In summary, the presence of a prominent lateral cnemial crest continuous with the fibular crest at the proximal end of the tibia in *Sinovenator changii* remains uncertain, and the validity of this character requires further investigation.

SDUST-V1062 displays clear differences from other troodontids of the Jehol Biota. It differs from *Mei* in having a mediolaterally flat proximal pubic shaft, whereas the proximal end of the pubic shaft is significantly compressed anteroposteriorly in *Mei* (Xu and Norell 2004; Gao et al. 2012). In SDUST-V1062, the shafts of metatarsals II and IV are nearly parallel in posterior view and do not contact each other. In *Mei*, however, metatarsals II and IV contact each other (Xu and Norell 2004). SDUST-V1062 differs from *Jinfengopteryx* by possessing a relatively short radius, approximately 65% of the humeral length, compared with 86% in *Jinfengopteryx* (Ji et al. 2005).

SDUST-V1062 can be distinguished from *Daliansaurus* by the presence of a small pedal ungual IV, with pedal ungual II being significantly larger than ungual IV, whereas pedal ungual IV is approximately the same size as pedal ungual II in *Daliansaurus* (Shen et al. 2017b). SDUST-V1062 differs from *Jianianhualong* in possessing a short pedal digit I, with the distal end of ungual I reaching only the proximal end of the distal condyles of metatarsal III. In contrast, pedal digit I is proportionally long, and the distal end of ungual I extends beyond the distal end of metatarsal III in *Jianianhualong*. In addition, the length ratio of pedal phalanx I-1 to metatarsal I is 0.7 in SDUST-V1062, whereas the ratio is 1.9 in *Jianianhualong* (Xu et al. 2017). Unlike in *Liaoningvenator*, manual phalanx I-1 and metacarpal II of SDUST-V1062 are subequal in length, whereas manual phalanx I-1 is longer than metacarpal II, and the length ratio of phalanx I-1 to metacarpal II is approximately 1.49 in *Liaoningvenator* (Shen et al. 2017a). SDUST-V1062 differs from *Sinusonasus* in having a subarctometatarsalian pes rather than the fully arctometatarsalian condition (Xu and Wang 2004).

As previously mentioned, SDUST-V1062 is attributed to *Sinovenator changii* rather than being used to erect a new taxon until more fossil material becomes available or more comprehensive studies are conducted.

Notable new morphologies observed in SDUST-V1062

SDUST-V1062 shows anatomical characteristics that distinguish it from other troodontids. In Late Cretaceous troodontids such as *Saurornithoides* (Norell et al. 2009), *Gobivenator* (Tsuihiji et al. 2014), and *Latenivenatrix* (Van der Reest and Currie 2017), the ambiens process at the proximal end of the pubis is clearly elongated anteroposteriorly and is longer than the ischial peduncle of the pubis (Fig. 17). However, because of the incomplete preservation of the pelvis, this feature is ambiguous in Early Cretaceous Jehol troodontids (Van der Reest and Currie 2017). Notably, the ambiens process appears to be absent in the holotype of *Sinovenator changii* (Fig. 17A), although this could result from preservation. In SDUST-V1062, the ambiens process is moderately developed, and its anteroposterior length is less than that of the ischial peduncle of the pubis (Fig. 17B), unlike the condition in *Gobivenator*, *Latenivenatrix*, and *Saurornithoides*. The moderately developed ambiens process of SDUST-V1062 possibly represents the incipient stage of elongation of the ambiens process in troodontids, revealing an evolutionary trend toward anteroposterior lengthening of the ambiens process within Troodontidae.

The ambiens process serves as the primary attachment site for M. ambiens and also bears attachment areas for M. obliquus abdominis and the pelvic ligaments (Hutchinson 2001; Rhodes et al. 2021). In dinosaurs, M. ambiens is one of the primary knee extensors (Allen et al. 2021), and the degree of development of its bony attachment directly governs the moment output of the hindlimb extensor complex and overall locomotor performance. Late Cretaceous troodontids possess anteroposteriorly elongated ambiens processes that lengthen the moment arm of M. ambiens, potentially improving their capacity for sustained running and weight-bearing. In contrast, the moderately developed ambiens process of SDUST-V1062 provides a shorter moment arm, which may imply relatively limited sprinting and locomotor performance compared with Late Cretaceous troodontids.

Paleogeographic significance of SDUST-V1062

In China, at least eight Early Cretaceous troodontid species have been reported, and most were reported from the Jehol Biota, except *Sinornithoides*, which was reported from the Ordos Basin (Russell and Dong 1993). *Sinovenator*, *Sinusonasus*, *Mei*, *Daliansaurus*, and *Liaoningvenator* were discovered in the Lower Cretaceous Yixian Formation at Lujiatun, western Liaoning; *Jianianhualong* was discovered in the Yixian Formation at Baicaigou, western Liaoning; and *Jinfengopteryx* was discovered in the Lower Cretaceous Qiaotou Formation at Fengning, Hebei Province. SDUST-V1062 was collected from Ningcheng, Inner Mongolia, and the faunal composition and lithological features of the fossil beds are the same as those of the Lujiatun Unit of the Yixian Formation at Beipiao, western Liaoning (Zhang et al. 2022). The new specimen of *Sinovenator* described here is the first record of a troodontid from the Jehol Biota in Inner Mongolia, which expands the geographical range of the troodontids of the Jehol Biota.

Body size variation within deinonychosaurians

Body size influences many aspects of animal biology, including physiology, ecology, life history, and energetics, and extreme variation in body size reflects substantial divergence in the underlying biological processes (Benson et al. 2017). Body size change has previously been investigated in theropod dinosaurs, including deinonychosaurians (Turner et al. 2007; Lee et al. 2014; Wang et al. 2021). An updated body size dataset (Suppl. material 3), expanded from Turner et al. (2007), was examined. Body size estimates were calculated using an empirical regression equation derived from femoral length. Among all measured specimens, only *Wulong* likely represents a juvenile individual, whereas all remaining specimens were identified as subadults or adults in their original published studies. The results of the body size analyses indicate that troodontids range from 0.54 to 2.82 m in body length and from 0.36 to 61.64 kg in body mass. Early Cretaceous troodontids display limited body size variation, with estimated body lengths ranging from 0.54 to 1.24 m. In contrast, Late Cretaceous troodontids exhibit far greater variation, with body length estimates spanning 0.57–2.82 m. Among Jehol troodontids, most species have a body length of approximately 1 m, except for *Mei* and *Jinfengopteryx* (Fig. 18), and SDUST-V1062 represents the largest known Jehol troodontid specimen (1.24 m and 4.53 kg). Body size estimates for dromaeosaurids range from 0.49 to 4.94 m in body length and from 0.26 to 368.70 kg in body mass. The body length of the largest dromaeosaurid is approximately 10.08 times that of the smallest, whereas this ratio is only approximately 5.22 in troodontids. This demonstrates that dromaeosaurids exhibit significantly greater size disparity than troodontids (Fig. 18). This pattern may reflect greater diversity in locomotion, ecological niches, or growth strategies in dromaeosaurids than in troodontids. A similar pattern is already evident in the Early Cretaceous Jehol Biota: the smallest known dromaeosaurid specimen (*Zhongjianosaurus*, 0.49 m) and troodontid specimen (*Mei*, 0.54 m) exhibit comparable body lengths, whereas the largest known dromaeosaurid specimen (STM 1-3, a subadult of *Tianyuraptor*, 1.82 m) attains a substantially greater body length than the largest troodontid specimen (SDUST-V1062, 1.24 m).

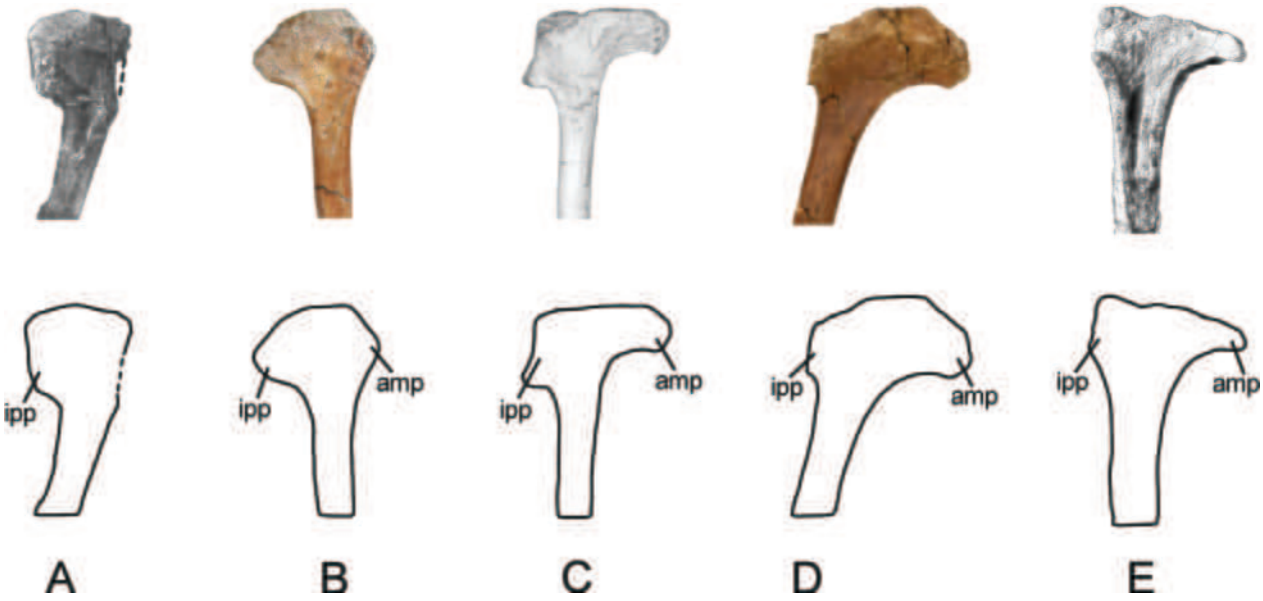

Figure 17. Proximal pubes of selected troodontids in lateral view. **A.** *Sinovenator* (IVPP V12615); **B.** SDUST-V1062; **C.** *Gobivenator*; **D.** *Latenivenatrix*; **E.** *Saurornithoides*. Abbreviations: amp, ambiens process; ipp, ischial peduncle of the pubis.

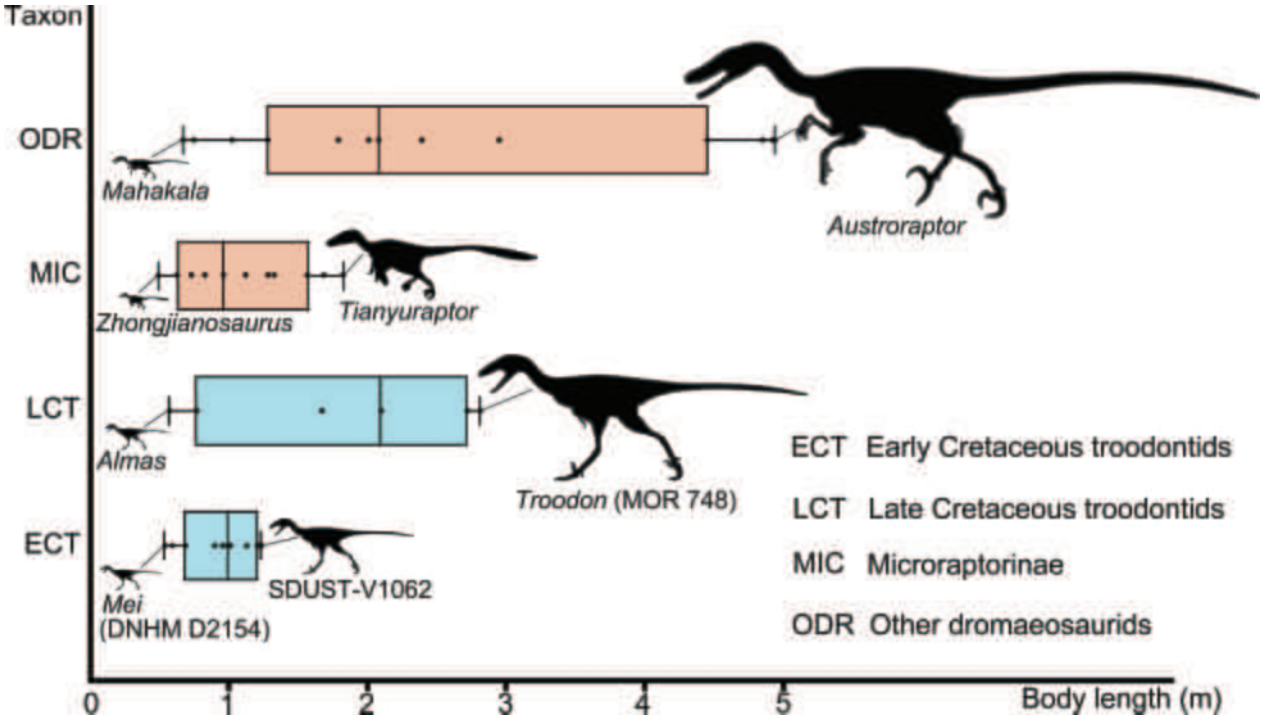

Figure 18. Boxplot of body length in deinonychosaurians.

Conclusion

SDUST-V1062 from the Yixian Formation of the Ningcheng Basin, Inner Mongolia, China, is the first record of a troodontid from the Jehol Biota in this area. Based on the presence of two pneumatic foramina on the lateral surface of the anterior cervical vertebrae, this specimen is referred to *Sinovenator changii*. The results of the phylogenetic analyses further corroborate this evolutionary inference. This finding expands the paleogeographic distribution of this species. Moreover, SDUST-V1062 shows a moderately developed pubic ambiens process, representing the first record of this feature in *Sinovenator changii*. This trait differs from the anteroposteriorly elongated pubic ambiens processes seen in Late Cretaceous troodontids, indicating a gradual evolutionary trend toward lengthening of the ambiens process within Troodontidae. Furthermore, body size comparisons within deinonychosaurians demonstrate substantially greater body size disparity among dromaeosaurids than among troodontids.

Acknowledgments

The authors thank Dr. Ya-Lei Yin (Shenyang Normal University, Shenyang, China) for his helpful discussions on the morphology of *Sinovenator*. The authors also thank Dr. Yu Peng (Zhejiang University, Hangzhou, China) for his assistance with the CT scanning of this fossil and Qiang Yang, Shurui Yang, Shuai Shao, Peng Yu, and Yuguo Yang (all from the Paleontological Museum of Liaoning, Shenyang, China) for their assistance with field excavations and fossil preparation. The authors also thank Dr. Emanuel Tschopp and Dr. James Logan King for reviewing the paper and providing insightful comments.

References

Allen VR, Kilbourne BM, Hutchinson JR (2021) The evolution of pelvic limb muscle moment arms in bird-line archosaurs. Science Advances 7: eabe2778. https://doi.org/10.1126/sciadv.abe2778

Barsbold R, Osmólska H, Kurzanov SM (1987) On a new troodontid (Dinosauria, Theropoda) from the Early Cretaceous of Mongolia. Acta Palaeontologica Polonica 32: 121–132. https://www.app.pan.pl/archive/published/app32/app32-121.pdf

Benson RBJ, Hunt G, Carrano MT, Campione N (2017) Cope's rule and the adaptive landscape of dinosaur body size evolution. Palaeontology 61: 13–48. https://doi.org/10.1111/pala.12329

Currie PJ, Dong ZM (2001) New information on Cretaceous troodontids (Dinosauria, Theropoda) from the People's Republic of China. Canadian Journal of Earth Sciences 38: 1753–1766. https://doi.org/10.1139/cjes-38-12-1753

Ezcurra MD (2024) Exploring the effects of weighting against homoplasy in genealogies of palaeontological phylogenetic matrices. Cladistics 40: 242–281. https://doi.org/10.1111/cla.12581

Fowler DW, Freedman EA, Scannella JB, Kambic RE (2011) The predatory ecology of *Deinonychus* and the origin of flapping in birds. PLoS ONE 6: e28964. https://doi.org/10.1371/journal.pone.0028964

Gao CL, Morschhauser EM, Varricchio DJ, Liu JY, Zhao B (2012) A second soundly sleeping dragon: new anatomical details of the Chinese troodontid *Mei long* with implications for phylogeny and taphonomy. PLoS ONE 7: e45203. https://doi.org/10.1371/journal.pone.0045203

Gianechini FA, Makovicky PJ, Apesteguía S, Cerda I (2018) Postcranial skeletal anatomy of the holotype and referred specimens of *Buitreraptor gonzalezorum* Makovicky, Apesteguía & Agnolín, 2005 (Theropoda, Dromaeosauridae), from the Late Cretaceous of Patagonia. PeerJ 6: e4558. https://doi.org/10.7717/peerj.4558

Goloboff PA, Catalano SA (2016) TNT version 1.5, including a full implementation of phylogenetic morphometrics. Cladistics 32: 221–238. https://doi.org/10.1111/cla.12160

Goloboff PA, Farris JS, Nixon KC (2008) TNT, a free program for phylogenetic analysis. Cladistics 24: 774–786. https://doi.org/10.1111/j.1096-0031.2008.00217.x

Hone DWE, Persons WS, Comber SCL (2021) New data on tail lengths and variation along the caudal series in the non-avialan dinosaurs. PeerJ 9: e10721. https://doi.org/10.7717/peerj.10721

Hutchinson JR (2001) The evolution of pelvic osteology and soft tissues on the line to extant birds (Neornithes). Zoological Journal of the Linnean Society 131: 123–168. https://doi.org/10.1006/zjls.2000.0254

Hwang SH, Norell MA, Ji Q, Gao KQ (2002) New specimens of *Microraptor zhaoianus* (Theropoda: Dromaeosauridae) from northeastern China. American Museum Novitates 3381: 1–44. https://doi.org/10.1206/0003-0082(2002)381<0001:NSOMZT>2.0.CO;2

Ji Q, Ji SA, Lu JC, You HL, Chen W, Liu YQ, Liu YX (2005) First avialian bird from China (*Jinfengopteryx elegans* gen. et sp. nov.). Geological Bulletin of China 24: 197–210. https://doi.org/10.12097/gbc.20050341

Kubota K, Kobayashi Y, Ikeda T (2024) Early Cretaceous troodontine troodontid (Dinosauria: Theropoda) from the Ohyamashimo Formation of Japan reveals the early evolution of Troodontinae. Scientific Reports 14: 16392. https://doi.org/10.1038/s41598-024-66815-2

Kurzanov SM, Osmólska H (1991) *Tochisaurus nemegtensts* gen. et sp. n., a new troodontid (Dinosauria, Theropoda) from Mongolia. Acta Palaeontologica Polonica 36: 69–76. https://www.app.pan.pl/archive/published/app36/app36-069.pdf

Lee MSY, Cau A, Naish D, Dyke GJ (2014) Sustained miniaturization and anatomical innovation in the dinosaurian ancestors of birds. Science 345: 562–566. https://doi.org/10.1126/science.1252243

Li JH, Pei R, Teng FF, Qiu H, Tagle R, Yan QQ, Wang Q, Chu XL, Xu X (2021) Micro-XRF study of the troodontid dinosaur *Jianianhualong tengi* reveals new biological and taphonomical signals. Atomic Spectroscopy 42: 1–11. https://doi.org/10.46770/AS.2021.01.001

Li Y, Feng YH, Hu XT, Zhou CF, Zhang HG (in press) The first LA-ICP-MS Zircon U-Pb age of Duanjiagou fossil site in Ningcheng, Inner Mongolia: revealing Lujiatun bed of the Jehol Group. Journal of Palaeogeography.

Makovicky PJ, Norell MA (2004) Troodontidae. In: Weishampel DB, Dodson P, Osmólska H (Eds) The Dinosauria, 2nd edn. University of California Press, Berkeley, 184–195. https://doi.org/10.1525/california/9780520242098.003.0011

Makovicky PJ, Norell MA, Clark JM, Rowe T (2003) Osteology and relationships of *Byronosaurus jaffei* (Theropoda: Troodontidae). American Museum Novitates 3402: 1–32. https://doi.org/10.1206/0003-0082(2003)402<0001:OAROBJ>2.0.CO;2

Napoli JG, Fabbri M, Ruebenstahl AA, O'Connor JK, Bhullar BAS, Norell MA (2025) Reorganization of the theropod wrist preceded the origin of avian flight. Nature 644: 699–705. https://doi.org/10.1038/s41586-025-09232-3

Norell MA, Hwang SH (2004) A troodontid dinosaur from Ukhaa Tolgod (Late Cretaceous Mongolia). American Museum Novitates 3446: 1–9. https://doi.org/10.1206/0003-0082(2004)446<0001:ATDFUT>2.0.CO;2

Norell MA, Makovicky PJ (1999) Important features of the dromaeosaurid skeleton II: information from newly collected specimens of *Velociraptor mongoliensis*. American Museum Novitates 3282: 1–45. http://hdl.handle.net/2246/3025

Norell MA, Clark JM, Turner AH, Makovicky PJ, Barsbold R, Rowe T (2006) A new dromaeosaurid theropod from Ukhaa Tolgod (Ömnögov, Mongolia). American Museum Novitates 3545: 1–51.

https://doi.org/10.1206/0003-0082(2006)3545[1:ANDTFU]2.0.CO;2

Norell MA, Makovicky PJ, Bever GS, Balanoff AM, Clark JM, Barsbold R, Rowe T (2009) A review of the Mongolian Cretaceous dinosaur *Saurornithoides* (Troodontidae: Theropoda). American Museum Novitates 3654: 1–63. https://doi.org/10.1206/648.1

O'Connor J, Clark A, Kuo PC, Kiat Y, Fabbri M, Shinya A, Beek CV, Lu J, Wang M, Hu H (2025) Chicago *Archaeopteryx* informs on the early evolution of the avian bauplan. Nature 641: 1201–1207. https://doi.org/10.1038/s41586-025-08912-4

Ostrom JH (1969) Osteology of *Deinonychus antirrhopus*, an unusual theropod from the Lower Cretaceous of Montana. Peabody Museum of Natural History, New Haven, 165 pp.

Ostrom JH (1976) *Archaeopteryx* and the origin of birds. Biological Journal of the Linnean Society 8: 91–182. https://doi.org/10.1111/j.1095-8312.1976.tb00244.x

Pei R (2015) New paravian fossils from the Mesozoic of East Asia and their bearing on the phylogeny of the Coelurosauria. PhD Thesis, Columbia University, New York.

Pei R, Li QG, Meng QJ, Gao KQ, Norell MA (2014) A new specimen of *Microraptor* (Theropoda: Dromaeosauridae) from the Lower Cretaceous of western Liaoning, China. American Museum Novitates 3821: 1–28. https://doi.org/10.1206/3821.1

Pei R, Li QG, Meng QJ, Norell MA, Gao KQ (2017a) New specimens of *Anchiornis huxleyi* (Theropoda: Paraves) from the Late Jurassic of northeastern China. Bulletin of the American Museum of Natural History 411: 1–67. https://doi.org/10.1206/0003-0090-411.1.1

Pei R, Norell MA, Barta DE, Bever GS, Pittman M, Xu X (2017b) Osteology of a new Late Cretaceous troodontid specimen from Ukhaa Tolgod, Ömnögovi Aimag, Mongolia. American Museum Novitates 3889: 1–47. https://doi.org/10.1206/3889.1

Pei R, Pittman M, Goloboff PA, Dececchi TA, Habib MB, Kaye TG, Larsson HCE, Norell MA, Brusatte SL, Xu X (2020) Potential for powered flight neared by most close avialan relatives, but few crossed its thresholds. Current Biology 30: 4033–4046. https://doi.org/10.1016/j.cub.2020.06.105

Pei R, Qin YY, Wen AS, Zhao Q, Wang Z, Liu ZM, Guo WLS, Liu P, Ye WM, Wang LY, Yin ZG, Dai RM, Xu X (2021) A new troodontid from the Upper Cretaceous Gobi Basin of Inner Mongolia, China. Cretaceous Research 130: 105052. https://doi.org/10.1016/j.cretres.2021.105052

Rhodes MM, Henderson DM, Currie PJ (2021) Maniraptoran pelvic musculature highlights evolutionary patterns in theropod locomotion on the line to birds. PeerJ 9: e10855. https://doi.org/10.7717/peerj.10855

Russell DA, Dong ZM (1993) A nearly complete skeleton of a new troodontid dinosaur from the Early Cretaceous of the Ordos Basin, Inner Mongolia, People's Republic of China. Canadian Journal of Earth Sciences 30: 2163–2173. https://doi.org/10.1139/e93-187

Shen CZ, Zhao B, Gao CL, Lu JC, Kundrát M (2017a) A new troodontid dinosaur (*Liaoningvenator curriei* gen. et sp. nov.) from the Early Cretaceous Yixian Formation in western Liaoning Province. Acta Geoscientica Sinica 38: 359–371. https://doi.org/10.3975/cagsb.2017.03.06

Shen CZ, Lu JC, Liu SZ, Kundrát M, Brusatte SL, Gao HL (2017b) A new troodontid from the Lower Cretaceous Yixian Formation of Liaoning Province, China. Acta Geologica Sinica (English Edition) 91: 763–780. https://doi.org/10.1111/1755-6724.13307

Shen CZ, Lu JC, Gao CL, Hoshino M, Uesugi K, Kundrát M (2017c) Forearm bone histology of the small theropod *Daliansaurus liaoningensis* (Paraves: Troodontidae) from the Yixian Formation, Liaoning, China. Historical Biology 31: 253–261. https://doi.org/10.1080/08912963.2017.1360296

Tschopp E, Upchurch P (2018) The challenges and potential utility of phenotypic specimen-level phylogeny based on maximum parsimony. Earth and Environmental Science Transactions of the Royal Society of Edinburgh 109: 301–323. https://doi.org/10.1017/S1755691018000877

Tsuihiji T, Barsbold R, Watabe M, Tsogtbaatar K, Chinzorig T, Fujiyama Y, Suzuki S (2014) An exquisitely preserved troodontid theropod with new information on the palatal structure from the Upper Cretaceous of Mongolia. Naturwissenschaften 101: 131–142. https://doi.org/10.1007/s00114-014-1143-9

Turner AH, Pol D, Clarke JA, Erickson GM, Norell MA (2007) A basal dromaeosaurid and size evolution preceding avian flight. Science 317: 1378–1381. https://doi.org/10.1126/science.1144066

Turner AH, Pol D, Norell MA (2011) Anatomy of *Mahakala omnogovae* (Theropoda: Dromaeosauridae), Tögrögiin Shiree, Mongolia. American Museum Novitates 3722: 1–66. https://doi.org/10.1206/3722.2

Turner AH, Makovicky PJ, Norell MA (2012) A review of dromaeosaurid systematics and paravian phylogeny. Bulletin of the American Museum of Natural History 371: 1–206. https://doi.org/10.1206/748.1

Van der Reest AJ, Currie PJ (2017) Troodontids (Theropoda) from the Dinosaur Park Formation, Alberta, with a description of a unique new taxon: implications for deinonychosaur diversity in North America. Canadian Journal of Earth Sciences 54: 919–935. https://doi.org/10.1139/cjes-2017-0031

Wang S, Zhang QY, Tan QW, Jiangzuo QG, Zhang HT, Tan L (2021) New troodontid theropod specimen from Inner Mongolia, China clarifies phylogenetic relationships of later-diverging small-bodied troodontids and paravian body size evolution. Cladistics 38: 59–82. https://doi.org/10.1111/cla.12467

Wellnhofer P (2009) *Archaeopteryx*: The Icon of Evolution. Verlag Dr. Friedrich Pfeil, Munich, 208 pp.

Wilson JA (1999) A nomenclature for vertebral laminae in sauropods and other saurischian dinosaurs. Journal of Vertebrate Paleontology 19: 639–653. https://doi.org/10.1080/02724634.1999.10011178

Wilson JA, D'Emic MD, Ikejiri T, Moacdieh EM, Whitlock JA (2011) A nomenclature for vertebral fossae in sauropods and other saurischian dinosaurs. PLoS ONE 6: e17114. https://doi.org/10.1371/journal.pone.0017114

Xu X (2002) Deinonychosaurian fossils from the Jehol Group of western Liaoning and the coelurosaurian evolution. PhD Thesis, Chinese Academy of Sciences, Beijing.

Xu X, Norell MA (2004) A new troodontid dinosaur from China with avian-like sleeping posture. Nature 431: 838–841. https://doi.org/10.1038/nature02898

Xu X, Wang XL (2004) A new troodontid (Theropoda: Troodontidae) from the Lower Cretaceous Yixian Formation of western Liaoning, China. Acta Geologica Sinica 78: 22–26. https://doi.org/10.1111/j.1755-6724.2004.tb00671.x

Xu X, Wang XL, Wu XC (1999) A dromaeosaurid dinosaur with a filamentous integument from the Yixian Formation of China. Nature 401: 262–266. https://doi.org/10.1038/45769

Xu X, Norell MA, Wang XL, Makovicky PJ, Wu XC (2002) A basal troodontid from the Early Cretaceous of China. Nature 415: 780–784. https://doi.org/10.1038/415780a

Xu X, Zhou ZH, Wang XL, Kuang XW, Zhang FC, Du XK (2003) Four-winged dinosaurs from China. Nature 421: 335–340. https://doi.org/10.1038/nature01342

Xu X, Tan QW, Sullivan C, Han FL, Dong X (2011) A short-armed troodontid dinosaur from the Upper Cretaceous of Inner Mongolia and its implications for troodontid evolution. PLoS ONE 6: e22916. https://doi.org/10.1371/journal.pone.0022916

Xu X, Zhao Q, Sullivan C, Tan QW, Sander M, Ma QY (2012) The taxonomy of the troodontid IVPP V10597 reconsidered. Vertebrata PalAsiatica 50: 140–150. https://www.vertpala.ac.cn/EN/abstract/abstract1199.shtml

Xu X, Han FL, Zhao Q (2014) Homologies and homeotic transformation of the theropod 'semilunate' carpal. Scientific Reports 4: 6042. https://doi.org/10.1038/srep06042

Xu X, Currie P, Pittman M, Xing LD, Meng QJ, Lu JC, Hu DY, Yu CY (2017) Mosaic evolution in an asymmetrically feathered troodontid dinosaur with transitional features. Nature Communications 8: 1–12. https://doi.org/10.1038/ncomms14972

Yin YL, Pei R, Zhou CF (2018) Cranial morphology of *Sinovenator changii* (Theropoda: Troodontidae) on the new material from the Yixian Formation of western Liaoning, China. PeerJ 6: e4977. https://doi.org/10.7717/peerj.4977

Yu CY, Watanabe A, Qin ZC, King JL, Witmer LM, Ma QY, Xu X (2024) Avialan-like brain morphology in *Sinovenator* (Troodontidae, Theropoda). Communications Biology 7: 1–10. https://doi.org/10.1038/s42003-024-05832-3

Yu DX, Pei R, Yin YL, Zhou CF (2022) The morphology and function of the manual digits of a troodontid from the Yixian Formation of western Liaoning, China. Historical Biology 36: 183–192. https://doi.org/10.1080/08912963.2022.2155149

Zanno LE, Varricchio DJ, O'Connor PM, Titus AL, Knell MJ (2011) A new troodontid theropod, *Talos sampsoni* gen. et sp. nov., from the Upper Cretaceous western interior basin of North America. PLoS ONE 6: e24487. https://doi.org/10.1371/journal.pone.0024487

Zhang HG, Yu DX, Feng YX, Pei R, Zhou CF (2022) A Lujiatun-like dinosaurian assemblage from the Jehol Biota of Ningcheng, Inner Mongolia, Northeast China. Acta Palaeontologica Polonica 67: 617–621. https://doi.org/10.4202/app.00975.2022

Zhang HG, Zhou CF, Luo ZX (2024a) A new symmetrodont mammal from the Early Cretaceous Jehol Biota of Ningcheng Basin, Inner Mongolia, Northeast China. Acta Palaeontologica Polonica 69: 315–327. https://doi.org/10.4202/app.01154.2024

Zhang HG, Yin YL, Pei R, Zhou CF (2024b) Early-diverging titanosauriform (Dinosauria, Sauropoda) teeth from the Lower Cretaceous Yixian Formation of southeastern Inner Mongolia, Northeast China. Acta Geologica Sinica (English Edition) 98: 303–310. https://doi.org/10.1111/1755-6724.15169

Additional information

Conflict of interest

The authors have declared that no competing interests exist.

Ethical statement

No ethical statement was reported.

Artificial Intelligence (AI) use

The authors accept full responsibility for the content of the manuscript, including the disclosure of any use of AI.
No AI tools were used in the preparation of this manuscript.

Funding

This work was supported by the International Partnership Program of Chinese Academy of Sciences (Grant no. 052GJHZ2024029GC), the Taishan Scholar Program of Shandong Province (Grant no. tstp20240514), and the National Natural Science Foundation of China (Grant nos. 42372031 and 42288201).

Author contributions

Conceptualization: RP, CFZ. Data curation: CFZ, RP. Funding acquisition: CFZ, RP. Investigation: DY, CFZ, RP. Supervision: RP, CFZ. Validation: CFZ, RP, DY. Visualization: DY, RP, CFZ. Writing - original draft: CFZ, RP, DY. Writing - review and editing: DY, HZ, RP, CFZ.

Author ORCIDs

D. Yu https://orcid.org/0009-0002-9704-057X
H. Zhang https://orcid.org/0009-0008-2587-0770
C.-F. Zhou https://orcid.org/0000-0002-3744-7573
R. Pei https://orcid.org/0000-0002-5954-0728

Data availability

A total of 2,501 TIFF slices forming a single image stack, along with the 3D models of the cervical vertebrae, have been deposited in ADMorph (http://dx.doi.org/10.12112/R.44.Fossil). Original X-ray projection data were not archived during CT data acquisition and therefore have not been deposited. The morphological matrix and tree files for the phylogenetic analyses can be accessed via MorphoBank (https://www.morphobank.org/permalink/?P6437). CT-rendered images of the proatlas, atlas, and axis; full topologies derived from the phylogenetic analyses; and the body size dataset for deinonychosaurians are provided in Suppl. materials of this article.

Supplementary material 1

CT-rendered images of proatlas, atlas, and axis of SDUST-V1062

Authors: Dongxiang Yu, Honggang Zhang, Chang-Fu Zhou, Rui Pei
Data type: jpg
Explanation note: (A, B) lateral view, (C) anterior view, (D) posterior view, (E) dorsal view, (F) ventral view. Abbreviations: ainc, atlantal intercentrum; anar, atlantal neural arch; ax, axis; ep, epipophysis; od, odontoid; paf, posterior articular facet of the centrum; proa, proatlas; spof, spinopostzygapophyseal fossa; spol, spinopostzygapophyseal laminae.

Link: https://doi.org/10.3897/sjp.145.196379.suppl1

Supplementary material 2

Full topologies of strict consensus trees and agreement subtrees recovered under equal weighting and implied weighting

Authors: Dongxiang Yu, Honggang Zhang, Chang-Fu Zhou, Rui Pei
Data type: zip

Link: https://doi.org/10.3897/sjp.145.196379.suppl2

Supplementary material 3

The body size dataset in deinonychosaurians

Authors: Dongxiang Yu, Honggang Zhang, Chang-Fu Zhou, Rui Pei
Data type: xlsx

Link: https://doi.org/10.3897/sjp.145.196379.suppl3